Neutrophil-to-hepatocyte communication via LDLR-dependent miR-223–enriched extracellular vesicle transfer ameliorates nonalcoholic steatohepatitis

Yong He,[1] Robim M. Rodrigues,[1] Xiaolin Wang,[1] Wonhyo Seo,[1] Jing Ma,[1] Seonghwan Hwang,[1] Yaojie Fu,[1] Eszter Trojnár,[2] Csaba Mátyás,[2] Suxian Zhao,[2] Ruixue Ren,[1] Dechun Feng,[1] Pal Pacher,[2] George Kunos,[3] and Bin Gao[1]

[1]Laboratory of Liver Diseases, [2]Laboratory of Cardiovascular Physiology and Tissue Injury, and [3]Laboratory of Physiologic Studies, National Institute on Alcohol Abuse and Alcoholism (NIAAA), NIH, Bethesda, Maryland, USA.

Neutrophil infiltration around lipotoxic hepatocytes is a hallmark of nonalcoholic steatohepatitis (NASH); however, how these 2 types of cells communicate remains obscure. We have previously demonstrated that neutrophil-specific microRNA-223 (miR-223) is elevated in hepatocytes to limit NASH progression in obese mice. Here, we demonstrated that this elevation of miR-223 in hepatocytes was due to preferential uptake of miR-223–enriched extracellular vesicles (EVs) derived from neutrophils as well other types of cells, albeit to a lesser extent. This selective uptake was dependent on the expression of low-density lipoprotein receptor (LDLR) on hepatocytes and apolipoprotein E (APOE) on neutrophil-derived EVs, which was enhanced by free fatty acids. Once internalized by hepatocytes, the EV-derived miR-223 acted to inhibit hepatic inflammatory and fibrogenic gene expression. In the absence of this LDLR- and APOE-dependent uptake of miR-223–enriched EVs, the progression of steatosis to NASH was accelerated. In contrast, augmentation of this transfer by treatment with an inhibitor of proprotein convertase subtilisin/kexin type 9, a drug used to lower blood cholesterol by upregulating LDLR, ameliorated NASH in mice. This specific role of LDLR and APOE in the selective control of miR-223–enriched EV transfer from neutrophils to hepatocytes may serve as a potential therapeutic target for NASH.

Introduction

Nonalcoholic fatty liver disease (NAFLD) is the leading cause of chronic liver disease and ranges from simple fatty liver to nonalcoholic steatohepatitis (NASH), cirrhosis, and hepatocellular carcinoma (1, 2). NASH is characterized microscopically by steatosis, hepatocyte damage, inflammatory cell infiltration, and pericellular fibrosis (1, 2). One of the hallmarks of NASH is neutrophil infiltration around lipotoxic hepatocytes, which is believed to promote liver injury and inflammation by producing reactive oxygen species (3, 4). However, neutrophils have also been shown to play a beneficial role in the resolution of liver fibrosis via the production of microRNA-223 (miR-223) that inhibits macrophage activation (5). miR-223 is expressed at the highest levels by neutrophils (6), followed by macrophages at approximately 10-times lower levels, whereas its levels are very low in hepatocytes (7). Thus, miR-223 is considered a neutrophil-specific miRNA (8). miR-223 serves as a key fine-tuner that controls excessive inflammatory responses and neutrophil activation (9). Previous studies suggest that miR-223 forms a negative feedback loop to ameliorate alcohol- or drug-induced liver injury by limiting neutrophil infiltration and acute neutrophilic responses (7, 10). However, non-myeloid functions of miR-223 remain largely unidentified. Interestingly, we have previously found that miR-223 is markedly elevated in hepatocytes in obese mice, which ameliorates NASH by inhibiting expression of proinflammatory and profibrotic genes in hepatocytes (11). Here, we found that the cellular source of the increased miR-223 in hepatocytes was immune cells, mainly neutrophils, but how neutrophils and hepatocytes communicate to result in miR-223 transfer has remained obscure.

Cell-to-cell communication via direct contact or through soluble factors is of vital importance for multicellular organisms. A recently identified form of intercellular communication is mediated via extracellular vesicles (EVs), which are membrane-bound, nanometer-sized vesicles that are released by cells under normal, stressed, or transformed conditions and subsequently taken up by recipient cells (12, 13). EVs are packaged with a variety of cargoes, including proteins, lipids, nucleic acids (e.g., miRNA), etc., which act as vectors of information in cell-to-cell communication (14). However, cell-specific generation and transfer of EVs and the biological processes affected by the transferred cargoes remain to be elucidated. Several cell-specific markers have been used to identify the source of EVs in the circulation. For example, cytochrome P450 family 2 subfamily member 1 (CYP2E1) and miR-122 have been identified in hepatocyte-derived EVs (15, 16), and miR-223 has been detected in neutrophil-derived EVs (17). But, so far it has not been possible to isolate cell-specific EVs from the circulation. Another unresolved issue is the cellular mechanisms involved in the uptake of EVs by recipient cells, although several endocytic pathways have been implicated in EV uptake, including endocytosis, micropinocytosis, phagocytosis, and lipid raft–mediated

Conflict of interest: The authors have declared that no conflict of interest exists.

Submitted: June 22, 2020; **Accepted:** November 25, 2020; **Published:** February 1, 2021.
Reference information: *J Clin Invest*. 2021;131(3):e141513.
https://doi.org/10.1172/JCI141513.

internalization (18). The mechanisms of EV uptake may vary by cell type, such as clathrin-dependent endocytosis in neurons (19), caveolin-dependent endocytosis in epithelial cells (20), and lipid raft–dependent endocytosis in tumor cells (21). In the current study, we provide evidence suggesting that the low-density lipoprotein receptor (LDLR) on hepatocytes is involved in selective uptake of neutrophil-derived, miR-223–enriched EVs in obese mice and serves to mitigate the progression of NAFLD.

LDLR is mainly expressed in the liver where it helps remove approximately 70% of circulating LDL by endocytosing cholesterol-enriched LDL. Interestingly, hepatocytes also produce an abundance of proprotein convertase subtilisin/kexin type 9 (PCSK9) that degrades LDLR and subsequently increases serum cholesterol. PCSK9 inhibitors (such as alirocumab) can prevent LDLR degradation and subsequently remove circulating LDL cholesterol (22). Alirocumab is currently an FDA-approved monoclonal antibody for the second-line treatment of hypercholesterolemia in people who cannot manage their cholesterol levels through lifestyle and statin therapy. LDLR exerts it functions via the binding of apolipoprotein B100 (APOB) and APOE (23). APOE, a high-affinity ligand for LDLR, is mainly produced by hepatocytes but is also generated by monocytes/macrophages, astrocytes, and vascular cells (24). In the current study, we demonstrate that neutrophils also express APOE, which is upregulated by fatty acid treatment. APOE is detected in neutrophil-derived EVs and is responsible for the selective uptake of miR-223–enriched EVs by hepatocytes. Deletion of *Apoe* in immune cells promotes NASH, partially due to less transfer of miR-223 in the liver. On the other hand, treatment with a PCSK9 inhibitor enhances the LDLR-dependent miR-223 transfer in hepatocytes and subsequently ameliorates NASH features in a murine model of NASH. Taken together, these observations suggest that neutrophil-to-hepatocyte communication via the selective uptake of neutrophil-derived circulating miR-223–enriched EVs in hepatocytes plays an important role in controlling the progression of NAFLD.

Results

Immune cell–derived miR-223 is selectively transferred into the liver, ameliorating NASH. Our previous study revealed that miR-223 was highly elevated in the liver (hepatocytes) of HFD-fed mice and in human NASH samples (11). Here, we found that this miR-223 elevation was specific to the liver and was not found in other organs of HFD-fed mice, as demonstrated in Figure 1A. miR-223 is one of the most abundant miRNAs in the circulation and is expressed at highest levels in neutrophils/myeloid cells but low levels in hepatocytes (7, 25). To define whether miR-223 in myeloid cells contributes to circulating and hepatic miR-223, we generated chimeric mice via bone marrow (BM) transplantation (Supplemental Figure 1A; supplemental material available online with this article; https://doi.org/10.1172/JCI141513DS1). We found that transplantation of miR-223 knockout (miR-223KO) BM into WT mice ($WT^{KO\ BM}$) resulted in an approximately 80% to 90% reduction in circulating and liver miR-223, whereas transplantation of WT BM into miR-223KO mice ($miR\text{-}223KO^{WT\ BM}$) fully restored miR-223 expression in both HFD-fed (Figure 1B) and control diet–fed (CD-fed) mice (Supplemental Figure 1B). Moreover, miR-223 in situ hybridization analyses demonstrated that, as expected, miR-223 was undetectable in the hepatocytes of miR-223KO mice transplanted with miR-223KO BM ($miR\text{-}223KO^{KO\ BM}$) after HFD feeding, while it was detected in hepatocytes of $miR\text{-}223KO^{WT\ BM}$ mice (Supplemental Figure 1C). To further confirm that miR-223 was indeed localized in hepatocytes of $miR\text{-}223KO^{WT\ BM}$ mice and not in infiltrating neutrophils or neutrophil remnants, we performed miR-223 in situ hybridization and costained the cell cytoskeleton marker F-actin (with Alexa Fluor–labeled phalloidin) and the neutrophil-specific marker myeloperoxidase (MPO). As shown in Figure 1C, miR-223 was indeed localized exclusively in the hepatocytes of $miR\text{-}223KO^{WT\ BM}$ mice and not in neutrophils or neutrophil remnants. Collectively, these data suggest that immune cell–derived miR-223 is the main source of circulating miR-223, which is then transferred into hepatocytes in HFD-fed mice.

The important role of this immune cell–derived miR-223 in ameliorating NASH was further confirmed in BM transplantation experiments. As illustrated in Figure 1, D–F and Supplemental Figure 2, $miR\text{-}223KO^{KO\ BM}$ mice had worse NASH phenotypes than $WT^{WT\ BM}$ mice, as demonstrated by measurement of serum alanine aminotransferase (ALT), liver inflammation, steatosis, and fibrosis, which is consistent with our previous data showing that miR-223KO mice were more susceptible to the development of NASH after HFD feeding (11). Interestingly, transplantation of WT BM ameliorated NASH in $miR\text{-}223KO^{WT\ BM}$ mice, while transplantation of miR-223KO BM exacerbated NASH in $WT^{KO\ BM}$ mice.

Evidence that miR-223–enriched EVs taken up by hepatocytes are primarily from neutrophils. The above data suggest that miR-223 in hepatocytes originates, at least in part, from immune cells, which prompted us to investigate whether this is due to EV transfer (26). miRNA-223 was originally reported to be expressed in myeloid cells where it is the most abundant miRNA and the main component of neutrophil-derived EVs (27), as confirmed in Supplemental Figure 3A. In addition, neutrophils are the major myeloid cells in the circulation, so circulating miR-223 is likely to be mainly derived from neutrophils, although other types of myeloid cells (e.g., macrophages) also express miR-223, albeit at approximately 10-times lower levels (Supplemental Figure 3B). To further determine whether neutrophils contribute to circulating miR-223, we performed neutrophil depletion experiments. Injection of anti-Ly6G or anti–Gr-1 antibodies has been widely used to deplete neutrophils; however, these approaches suffer from limitations of low efficiency or specificity, especially during chronic depletion (28). Indeed, we found that treatment of HFD-fed mice with anti–Gr-1 antibody for 2 weeks only slightly reduced circulating neutrophils (data not shown). A recent paper reported that a combination of anti-Ly6G antibody and anti-rat secondary antibody enhanced neutrophil elimination and reduced neutrophil prevalence, resulting in more efficient and specific chronic neutrophil depletion (29). By using this combined treatment protocol, we found that circulating and hepatic neutrophils were reduced by approximately 30% and 20%, respectively (Figure 2, A and B, and Supplemental Figure 3, C and D). We did not achieve approximately 80% circulating neutrophil depletion as described in the original paper (29), and it is not clear whether this difference in depletion efficiency was due to our use of HFD-fed mice as compared with chow-fed mice used in the original paper (29). The approximately 30% reduction in circulating neutrophils was paralleled by a similar, approximate-

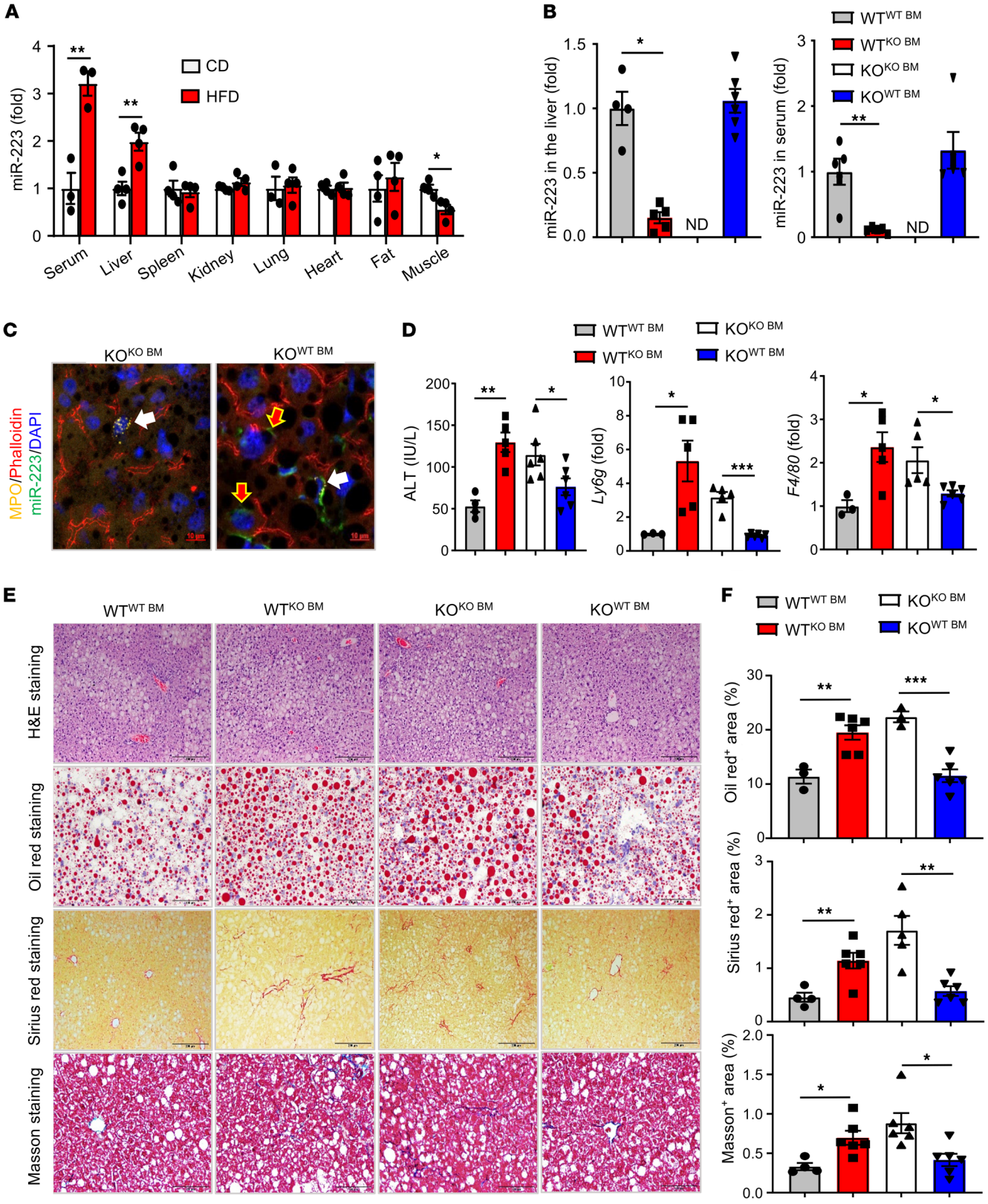
A
miR-223 (fold)
CD
HFD
Serum
Liver
Spleen
Kidney
Lung
Heart
Fat
Muscle
B
miR-223 in the liver (fold)
ND
miR-223 in serum (fold)
WTWT BM
WTKO BM
KOKO BM
KOWT BM
C
KOKO BM
KOWT BM
MPO/Phalloidin
miR-223/DAPI
D
ALT (IU/L)
Ly6g (fold)
F4/80 (fold)
E
H&E staining
Oil red staining
Sirius red staining
Masson staining
F
Oil red+ area (%)
Sirius red+ area (%)
Masson+ area (%)

Figure 1. Immune cell–derived miR-223 is selectively transferred into the liver (hepatocytes), ameliorating NASH. (**A**) C57BL/6J mice were fed HFD or CD for 3 months. Serum and different organ samples were collected for the measurement of miR-223 levels (n = 3–4). (**B**–**F**) WT and miR-223KO mice were transplanted with WT or miR-223KO mouse bone marrow (BM). Two months later, these mice were subjected to HFD feeding for 3 months (n = 4–6). (**B**) Serum and liver tissue samples were collected for miR-223 measurement. (**C**) Frozen liver tissue sections from HFD-fed mice were analyzed by miR-223 in situ hybridization along with immunofluorescence staining of neutrophil marker MPO and cell cytoskeleton marker F-actin that was detected by using Alexa Fluor–phalloidin. Representative images of miR-223 expression (green), MPO (yellow), phalloidin (red), and nuclei (DAPI, blue) are shown. White arrows indicate MPO$^+$ neutrophils (left panel) or miR-223$^+$MPO$^+$ neutrophils (right panel). Red arrows indicate miR-223$^+$ hepatocytes. Scale bars: 10 μm. (**D**) Serum ALT was measured (left panel). RT-qPCR analyses of liver *Ly6g* and *F4/80* mRNA levels (right panel). (**E**) Representative images of H&E staining (scale bars: 200 μm), Oil red staining (scale bars: 100 μm), Sirius red staining (scale bars: 200 μm), and Masson's trichrome staining (scale bars: 100 μm) of liver tissue sections are shown. (**F**) Oil red$^+$ area and fibrotic area per field were quantified. Values represent mean ± SEM. $^*P < 0.05$, $^{**}P < 0.01$, $^{***}P < 0.001$, as determined by 2-tailed Student's t test for comparing 2 groups (**A**, **B**, **D**, and **F**). ND, not detectable. The superscript characters shown for transplanted mice indicate the donor mouse BM.

ly 30% reduction in serum miR-223 levels (Figure 2A), suggesting that neutrophils are the major source of circulating miR-223. Additionally, miR-223 in situ hybridization analyses revealed that miR-223 levels were also reduced in hepatocytes after combined antibody injection (Figure 2B and Supplemental Figure 3E). Finally, combined antibody treatment did not alter serum ALT levels but increased hepatic expression of miR-223 target genes as well as some inflammatory, fibrogenic genes in HFD-fed mice (Figure 2C and Supplemental Figure 3F).

To test whether miR-223 is transferred directly from neutrophils into hepatocytes, we performed several experiments. First, coculture with WT neutrophils, but not with miR-223KO neutrophils, selectively increased the levels of miR-223 in AML12 mouse hepatocytes (Figure 2D and Supplemental Figure 4, A and B). Second, miR-223 expression was detected in miR-223KO hepatocytes after coculture with WT neutrophils (Figure 2E). Third, locally generated, primary miR-223 (pri-miR-223) was undetectable in hepatocytes before or after coculture (data not shown). Collectively, these data suggest that the increased miR-223 in hepatocytes after coculture is due to the direct transfer of miR-223 from neutrophils to hepatocytes rather than the upregulation of pri-miR-223 expression.

To further investigate whether EV-mediated transfer is the primary route of miR-223 transfer from neutrophils to hepatocytes, we first validated and characterized EVs isolated from neutrophils by using NanoSight tracking and detecting EV markers including CD63, ALIX, and HSP70 (Supplemental Figure 4, C and D). Because it is well known that neutrophils become apoptotic after in vitro culture, which may affect EV release, we examined neutrophil apoptosis and found approximately 5% dead neutrophils after short-term (6-hour) culture (Supplemental Figure 4E), suggesting that apoptosis is probably not the major mechanism affecting EV release during short-term culture. In addition, the levels of miR-223 in neutrophils had a decreasing trend after 6-hour culture (Supplemental Figure 4F). Moreover, treatment with the EV release inhibitor GW4869 markedly reduced the abundance of miR-223 in supernatant after 6-hour incubation (Supplemental Figure 4G). Interestingly, GW4869 also significantly suppressed miR-223 transfer from neutrophils to hepatocytes in coculture experiments (Figure 2F). Furthermore, we found that hepatocytes were able to take up fluorescently labeled neutrophil-derived EVs in vitro in coculture experiments and in vivo via the injection of EVs; however, this uptake was not observed when 0.1% Triton–lysed neutrophil-derived EVs were used (Supplemental Figure 4H). Most importantly, miR-223 in situ hybridization detected miR-223 expression in hepatocytes of miR-223KO mice after the injection of neutrophil-derived EVs but not Triton-lysed neutrophil-derived EVs (Figure 2G). Finally, hepatocytes can also take up fluorescently labeled macrophage-derived EVs (Supplemental Figure 4I).

All the above data support the conclusion that hepatocytes can incorporate miR-223 via the transfer of miR-223–enriched EVs originating from neutrophils and, to a lesser extent, macrophages.

Neutrophil-derived, miR-223–enriched EV uptake in lipotoxic hepatocytes is partially dependent on LDLR in vitro and in vivo. Because HFD feeding augments miR-223 transfer from immune cells into hepatocytes in mice (Figure 1 and Supplemental Figure 1), we wondered whether free fatty acids (FFAs), which are elevated during HFD feeding, enhance such a transfer of miR-223. To test this hypothesis, we treated AML12 hepatocytes with palmitic acid (PA) and then cocultured them with neutrophils. As illustrated in Figure 3A, in the presence of neutrophils, PA-pretreated hepatocytes expressed much higher levels of miR-223 than vehicle-treated hepatocytes, whereas PA treatment alone in the absence of neutrophils did not affect the basal level of miR-223 in hepatocytes. Next, we asked whether the increased transfer of miR-223 in PA-pretreated hepatocytes was mediated via neutrophil-derived, miR-223–enriched EVs. We found that PA-pretreated hepatocytes took up much more fluorescently labeled neutrophil-derived EVs (those containing miR-223) than vehicle-pretreated control hepatocytes (Figure 3, B and C). To understand why PA-pretreated hepatocytes take up more EVs, we examined the expression of several endocytosis-related genes in hepatocytes and found that among many of the genes examined, only LDLR expression was significantly upregulated after PA treatment (Figure 3D). Moreover, fluorescently labeled EVs and LDLR were colocalized in hepatocytes, which was markedly enhanced after PA treatment (Figure 3E).

Next, we examined the role of hepatocyte LDLR in uptake of neutrophil-derived miR-223–enriched EVs by using *Ldlr*-KO mice or hepatocytes. As illustrated in Figure 4, A and B, *Ldlr*-KO hepatocytes and *Ldlr*-KO mouse livers took up much fewer fluorescently labeled neutrophil-derived EVs than their WT counterparts in vitro and in vivo, respectively. Furthermore, knockout or knockdown of *Ldlr* in hepatocytes suppressed miR-223 transfer from neutrophils to vehicle- or PA-pretreated hepatocytes after coculture with neutrophils without affecting the basal levels of miR-223 in hepatocytes in the absence of neutrophils (Figure 4C). These data suggest that LDLR is involved in hepatocyte uptake of neutrophil-derived miR-223–enriched EVs in vitro. To test whether this LDLR-mediated uptake is functional in vivo, we examined hepatic and serum miR-223 levels and quantified the circulating EV numbers in WT and *Ldlr*-KO mice. As illustrated in Figure

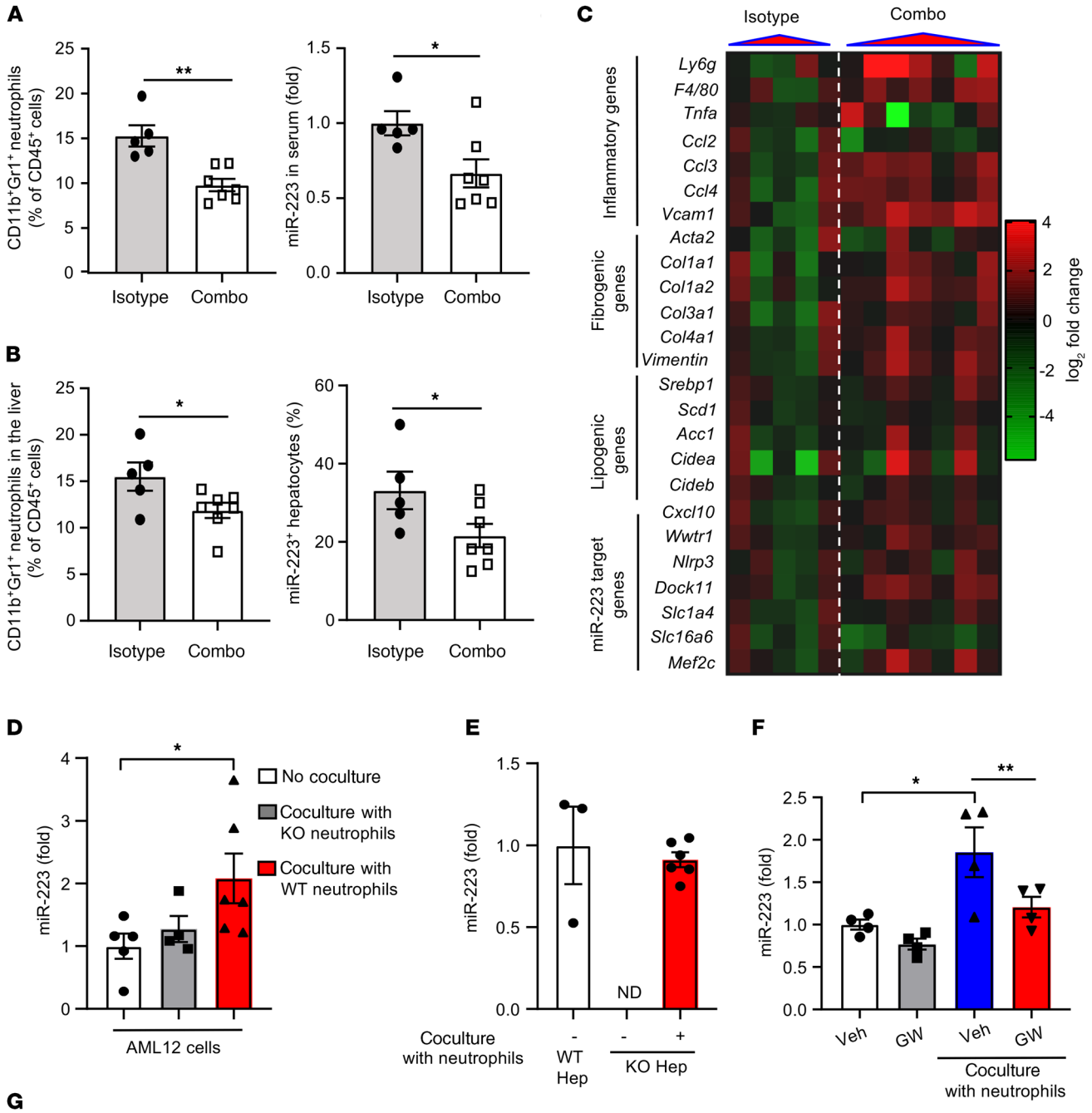
A
CD11b+Gr1+ neutrophils (% of CD45+ cells)
Isotype
Combo
miR-223 in serum (fold)
B
CD11b+Gr1+ neutrophils in the liver (% of CD45+ cells)
miR-223+ hepatocytes (%)
C
Isotype
Combo
Inflammatory genes
Ly6g
F4/80
Tnfa
Ccl2
Ccl3
Ccl4
Vcam1
Fibrogenic genes
Acta2
Col1a1
Col1a2
Col3a1
Col4a1
Vimentin
Lipogenic genes
Srebp1
Scd1
Acc1
Cidea
Cideb
miR-223 target genes
Cxcl10
Wwtr1
Nlrp3
Dock11
Slc1a4
Slc16a6
Mef2c
log2 fold change
D
miR-223 (fold)
No coculture
Coculture with KO neutrophils
Coculture with WT neutrophils
AML12 cells
E
miR-223 (fold)
ND
Coculture with neutrophils
WT Hep
KO Hep
F
miR-223 (fold)
Veh
GW
Coculture with neutrophils
G
miR-223
Phalloidin
DAPI
Merge
EV injection
Triton-lysed EV injection

Figure 2. Neutrophils transfer miR-223 to hepatocytes via EVs. (**A**–**C**) WT mice were fed HFD for 2.5 months, and then daily intraperitoneally injected with isotype antibody or combined (Combo) antibodies (rat anti–mouse Ly6G antibody and anti-rat secondary antibody). Liver, circulating blood leukocytes, and serum samples were collected 24 hours after the last injection (n = 5 in isotype group, n = 7 in combined group). (**A**) The percentage of circulating neutrophils ($CD11b^+Gr\text{-}1^+/CD45^+$ cells), and serum miR-223 levels were quantified. (**B**) The percentage of liver neutrophils ($CD11b^+Gr\text{-}1^+/CD45^+$ cells) and the percentage of $miR\text{-}223^+$ hepatocytes (which were detected by miR-223 in situ hybridization) were quantified. (**C**) RT-qPCR analyses of inflammatory, fibrogenic, and miR-223 target genes in the liver samples. (**D**) Mouse hepatocyte line AML12 cells were cocultured with WT or miR-223KO neutrophils for 6 hours, and then miR-223 in AML12 cells was measured. (**E**) Primary WT or miR-223KO hepatocytes were cocultured with neutrophils for 6 hours, and miR-223 in hepatocytes was then measured. (**F**) AML12 cells were cocultured with neutrophils in the presence of vehicle or EV release inhibitor GW4869 (20 nM) for 6 hours, and miR-223 levels in AML12 cells were then measured. (**G**) Neutrophilic EVs were lysed by using 0.1% Triton X-100 for 30 minutes at room temperature. Neutrophil-derived EVs (250 μg/mouse) pretreated with or without 0.1% Triton were intravenously injected into miR-223KO mice for 4 hours. Hepatic miR-223 was detected by in situ hybridization. Representative images of miR-223 (green), phalloidin (red), and nuclei (DAPI, blue) are shown. Scale bars: 10 μm. Values represent means ± SEM from 3–4 independent experiments. $^*P < 0.05$, $^{**}P < 0.01$. Significance was determined by a 2-tailed Student's t test for comparing 2 groups (**A** and **B**) or 1-way ANOVA followed by Tukey's post hoc test for multiple groups (**D** and **F**). ND, not detectable.

4D, after HFD feeding, hepatic miR-223 levels were significantly upregulated in WT mice, but such hepatic miR-223 upregulation was blunted in *Ldlr*-KO mice, which is consistent with higher hepatic expression of miR-223 target genes (*Cxcl10*, *Nlrp3*, *Dock11*, *Slc1a4*, *Slc16a6*, and *Mef2c*) in HFD-fed *Ldlr*-KO mice compared with WT mice (Supplemental Figure 5). The reduced hepatic miR-223 in HFD-fed *Ldlr*-KO mice was likely due to reduced miR-223–enriched EV transfer because serum miR-223 and EV levels were higher in these mice than in WT mice (Figure 4E). Interestingly, in CD-fed groups, hepatic miR-223 levels and serum EV numbers were comparable between WT and *Ldlr*-KO mice, while serum miR-223 levels were lower in *Ldlr*-KO mice than in WT mice (Figure 4, D and E).

Finally, because CD36 plays an important role in cellular FFA uptake (30) and our above data revealed that PA induced hepatocytes to take up EVs, we wondered whether CD36 also contributes to FFA-mediated promotion of EV uptake by hepatocytes. Our data in Supplemental Figure 6, A and B, demonstrate that CD36 contributed to FFA uptake but not EV uptake by hepatocytes, suggesting CD36 is not involved in EV uptake.

Restoration of hepatic miR-223 ameliorates NASH in HFD-fed Ldlr-KO mice. Previous studies reported that *Ldlr*-KO mice developed NASH features after feeding NASH-inducing diets (high fat and high cholesterol; refs. 31, 32). Here, we found that *Ldlr*-KO mice were more susceptible to HFD-induced NASH phenotypes as demonstrated in Supplemental Figure 7, A–D, which shows that after HFD feeding, *Ldlr*-KO mice had higher levels of ALT, greater steatosis, liver fibrosis, and inflammation, as well as higher levels of the Mallory-Denk body marker p62 than WT mice. Because HFD-fed *Ldlr*-KO mice had reduced hepatic miR-223, which is known to ameliorate NASH (11), we wondered whether the severe NASH phenotypes in *Ldlr*-KO mice were partially due to the reduction of hepatic miR-223. To answer this question, we restored hepatic miR-223 expression in HFD-fed *Ldlr*-KO mice and found that overexpression of hepatic miR-223 markedly ameliorated steatosis, fibrosis, and NAFLD activity score (NAS), with a trend toward reduction of serum ALT levels in HFD-fed *Ldlr*-KO mice (Figure 5A and Supplemental Figure 8, A–C). Moreover, RT-qPCR analyses showed that hepatic levels of a macrophage marker (*F4/80*), inflammatory genes, fibrogenic genes, lipogenic genes, and miR-223 target genes were decreased in *Ldlr*-KO mice after restoration of hepatic miR-223 (Figure 5B).

PA induces neutrophils to release APOE-enriched EVs. The above data suggest that PA induces hepatocytes to take up neutrophil-derived EVs via the upregulation of LDLR expression. Conversely, we asked whether PA also affects neutrophil production of EVs and expression of LDLR-binding proteins such as APOB and APOE in EVs. Our data revealed that treatment of neutrophils with PA enhanced the release of EVs (Supplemental Figure 9A) and upregulated miR-223 expression in neutrophils and neutrophil-derived EVs (Figure 6A). Interestingly, *Apoe* mRNA was detected in neutrophils, which was lower than that in hepatocytes, but *Apob* mRNA was undetectable in neutrophils (Supplemental Figure 9B). Furthermore, PA markedly upregulated *Apoe* mRNA and purine-rich PU-box–binding protein 1 (PU.1) (Figure 6B), an important transcription factor that regulates miR-223 expression and is controlled by APOE (33, 34). Moreover, APOE protein levels were detected in neutrophils and neutrophil-derived EVs, which were further increased after PA treatment (Figure 6C).

Neutrophil-derived, miR-223–enriched EV uptake by hepatocytes is partially dependent on neutrophil APOE in vitro and in vivo, thus ameliorating NASH. To further explore the intracellular trafficking of APOE in EVs, we assessed the colocalization of APOE with the early endosome marker early endosome antigen 1 (EEA1), the EV marker CD63, and the late endosome marker Ras-related protein Rab-7 (RAB7), and found that APOE was colocalized with these markers in neutrophils after PA treatment (Figure 6D). To define the critical role of neutrophil APOE in EV uptake by hepatocytes, we performed several experiments. Firstly, EVs were purified from the supernatants of cultured WT and *Apoe*-KO neutrophils (these cells were cultured in serum-free medium and contained few lipoprotein particles) and labeled with the red fluorescent dye DiD. We then incubated these DiD-labeled EVs with hepatocytes and found that *Apoe*-KO EVs were much less effectively taken up by AML12 cells or primary hepatocytes than WT EVs (Figure 6E). Secondly, we examined the role of APOE in promoting hepatocytic uptake of neutrophil-derived miR-223 EVs in vivo. As illustrated in Supplemental Figure 10A, in the CD-fed group, hepatic miR-223 levels were lower in *Apoe*-KO mice than in WT mice, while serum miR-223 had a trend toward higher levels in *Apoe*-KO mice compared with WT mice, although it did not reach statistical significance. In the HFD-fed groups, hepatic miR-223 levels had a decreasing trend in *Apoe*-KO mice compared with WT mice, while miR-223 levels in serum EVs showed an increasing trend in *Apoe*-KO mice. Furthermore, RT-qPCR analyses demonstrated that hepatic expression of inflammatory and fibrogenic genes and miR-223 target genes was higher in *Apoe*-KO mice compared with WT mice after HFD feeding (Supplemental Figure 10B). To better understand

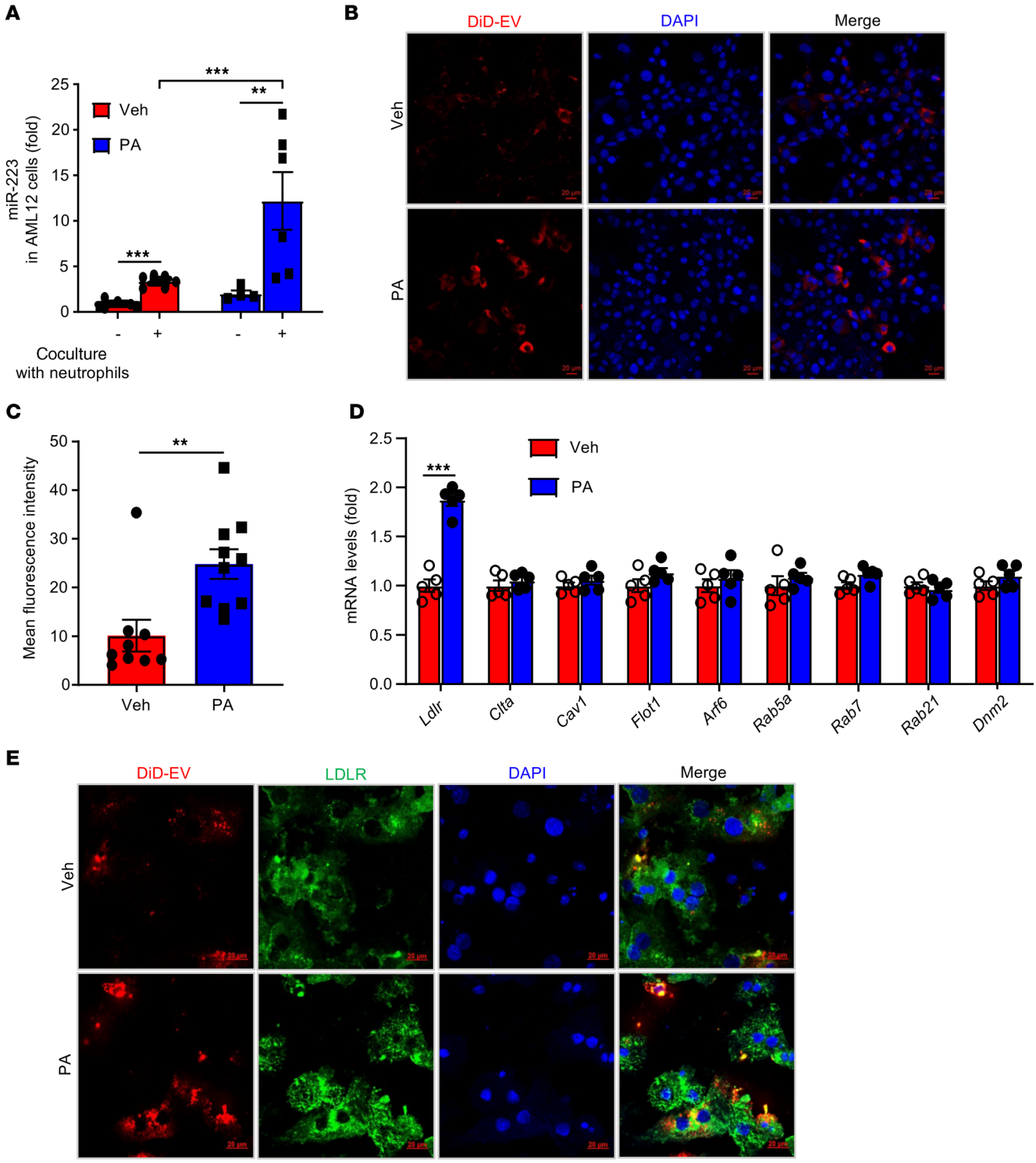

Figure 3. Fatty acid (e.g., palmitic acid [PA]) promotes neutrophil transfer of miR-223 to hepatocytes. (**A**) After pretreatment with PA (0.3 mM) for 18 hours, AML12 cell medium was replaced with fresh serum-free medium and the cells cocultured with neutrophils for another 6 hours. miR-223 levels in AML12 cells were measured by RT-qPCR. (**B** and **C**) AML12 cells were pretreated with vehicle or PA (0.3 mM) for 18 hours, followed by incubating with DiD-labeled neutrophil-derived EVs for 24 hours. Representative images of DiD fluorescence (red) and nuclei (DAPI, blue) are shown in panel **B**, and mean fluorescence intensity per cell is quantified in panel **C**. Scale bars: 20 μm. (**D**) AML12 cells were treated with vehicle or PA (0.3 mM) for 3 hours, and analyzed by RT-qPCR for several endocytosis-related genes. (**E**) AML12 cells were pretreated with vehicle or PA (0.3 mM) for 18 hours, followed by incubating with the DiD-labeled neutrophil-derived EVs for 24 hours and staining with an anti-LDLR antibody. Representative images of DiD fluorescence (red), LDLR immunofluorescence (green), and nuclei (DAPI, blue) are shown. Scale bars: 20 μm. Values represent means ± SEM from 3–4 independent experiments. $^{**}P < 0.01$, $^{***}P < 0.001$. Significance was determined by 1-way ANOVA followed by Tukey's post hoc test for multiple groups (**A**) and a 2-tailed Student's *t* test for comparing 2 groups (**C** and **D**). ND, not detectable.

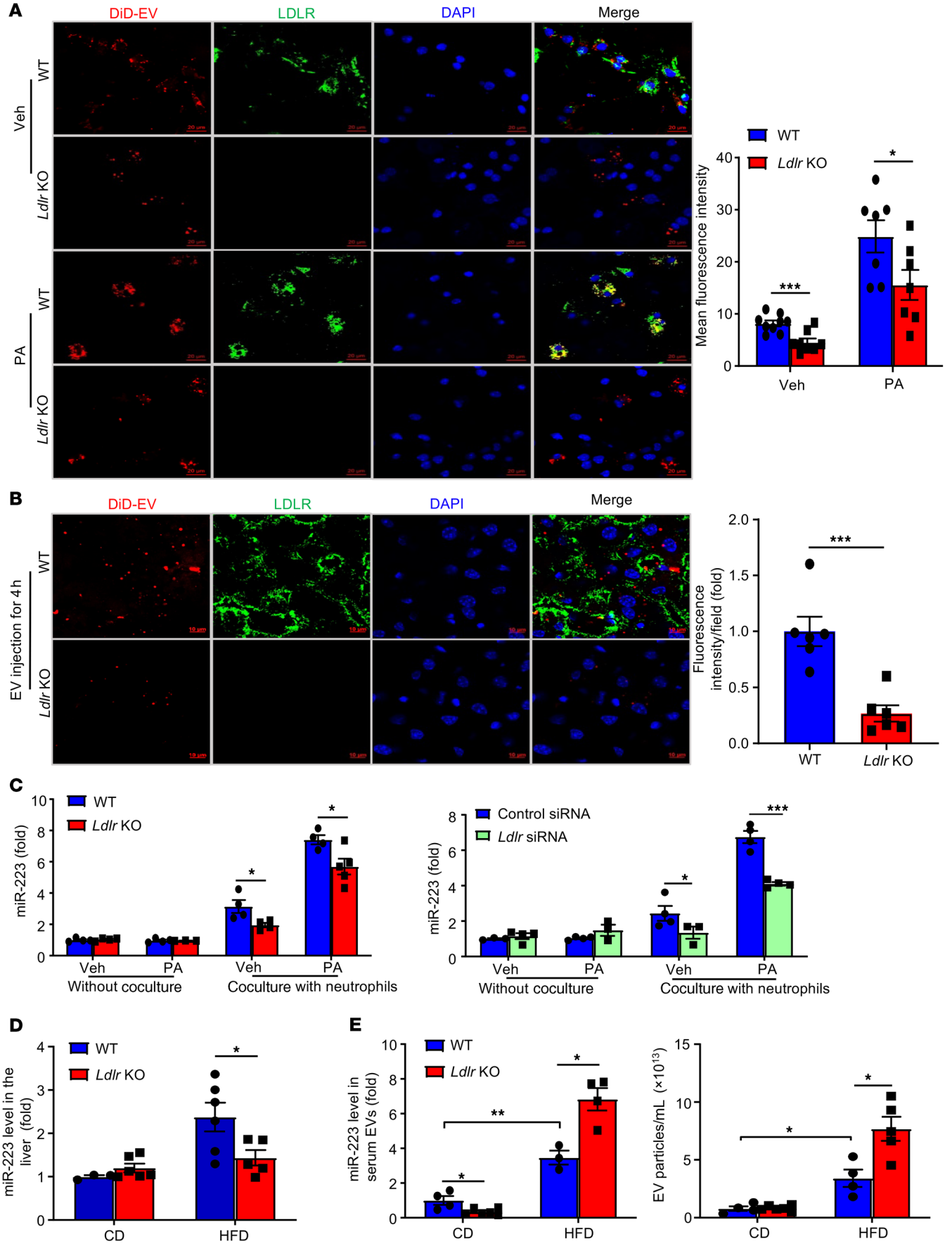
A
DiD-EV
LDLR
DAPI
Merge
Veh
PA
WT
Ldlr KO
Mean fluorescence intensity
WT
Ldlr KO
Veh
PA
B
EV injection for 4h
Fluorescence intensity/field (fold)
C
miR-223 (fold)
Without coculture
Coculture with neutrophils
Control siRNA
Ldlr siRNA
D
miR-223 level in the liver (fold)
CD
HFD
E
miR-223 level in serum EVs (fold)
EV particles/mL (×10^13)

Figure 4. Neutrophil-derived, miR-223–enriched EV uptake in lipotoxic hepatocytes is partially dependent on LDLR. (**A**) After pretreatment with vehicle or PA (0.3 mM) for 18 hours, WT and *Ldlr*-KO hepatocytes were cultured with fresh serum-free medium and incubated with DiD-labeled neutrophil-derived EVs, followed by performing immunofluorescence staining. Representative images of DiD (red), LDLR (green), and nuclei (DAPI, blue) are shown, and mean fluorescence intensity per cell was quantified. Scale bars: 20 μm. (**B**) DiD-labeled neutrophil-derived EVs were intravenously injected into WT and *Ldlr*-KO mice for 4 hours. Representative images of DiD (red), LDLR (green), and nuclei (blue) in the liver are shown, and relative fluorescence intensity per field was quantified. Scale bars: 10 μm. (**C**) In the left panel, after pretreatment with vehicle or PA (0.3 mM) for 18 hours, WT and *Ldlr*-KO hepatocyte cell medium was replaced with fresh serum-free medium and the cells cocultured with or without neutrophils for another 6 hours. miR-223 levels in hepatocytes were measured by RT-qPCR. In the right panel, AML12 cells were transfected with control or *Ldlr* siRNA for 24 hours, followed by treatment with vehicle or PA for 18 hours. AML12 cell medium was then replaced with fresh serum-free medium and the cells cocultured with or without neutrophils for another 6 hours. miR-223 levels in AML12 cells were measured by RT-qPCR. (**D** and **E**) WT and *Ldlr*-KO mice were fed CD or HFD for 3 months. Liver tissue samples were collected for the measurement of miR-223 (**D**) (n = 3–6). Serum samples were collected for EV isolation, and miR-223 in EVs and EV numbers were measured (**E**). Values represent means ± SEM. *P < 0.05, **P < 0.01, ***P < 0.001. Significance was determined by a 2-tailed Student's t test for comparing 2 groups (**A**–**D**) or 1-way ANOVA followed by Tukey's post hoc test for multiple groups (**E**).

the function of APOE in neutrophils and because *Apoe* global KO mice had a more severe NASH phenotype than WT mice after HFD feeding, which may affect miR-223 EV production and transfer, we generated chimeric mice to deplete *Apoe* expression in immune cells by transplanting *Apoe*-KO BM cells into WT mice (Supplemental Figure 11). As illustrated in Figure 7A, in the CD-fed mice, hepatic miR-223 expression was comparable between $WT^{WT\ BM}$ and $WT^{KO\ BM}$ mice, whereas in HFD-fed mice, hepatic miR-223 expression was much lower in $WT^{KO\ BM}$ mice than in $WT^{WT\ BM}$ mice (Figure 7A). The observed reduction in hepatic miR-223 is functional because HFD-fed $WT^{KO\ BM}$ mice had worse NASH phenotypes and higher hepatic expression of miR-223 target genes than HFD-fed $WT^{WT\ BM}$ mice. As illustrated in Figure 7, B–D, compared with HFD-fed $WT^{WT\ BM}$ mice, HFD-fed $WT^{KO\ BM}$ mice had higher levels of serum ALT (Figure 7B) and greater liver steatosis and fibrosis, as demonstrated by histological analyses of H&E staining, Sirius red staining, and immunostaining analysis of α-smooth muscle actin (α-SMA) (Figure 7C). Moreover, RT-qPCR analyses showed that inflammatory cell markers, inflammatory genes, fibrogenic genes, lipogenic genes, and miR-223 target genes were higher in HFD-fed $WT^{KO\ BM}$ mice than in HFD-fed $WT^{WT\ BM}$ mice (Figure 7D).

Treatment with the PCSK9 inhibitor alirocumab enhances the LDLR-dependent miR-223 transfer into hepatocytes and ameliorates NASH. The PCSK9 inhibitor alirocumab can prevent LDLR degradation and subsequently upregulate LDLR expression in hepatocytes (22, 35). Thus, we wondered whether treatment with the PCSK9 inhibitor alirocumab enhances the uptake of neutrophil-derived, miR-223 EVs by hepatocytes via the upregulation of LDLR protein expression. As illustrated in Figure 8A, treatment with alirocumab upregulated LDLR protein expression in hepatocytes and significantly enhanced miR-223 transfer after coculture with neutrophils, whereas alirocumab alone did not affect miR-223 expression in hepatocytes.

Because alirocumab treatment enhances LDLR-dependent miR-223–enriched EV transfer, which ameliorates NASH, we wondered whether such treatment protects against NASH progression. Given that HFD feeding alone induces very mild steatohepatitis and minimal fibrosis in mice (36), the beneficial effect of alirocumab treatment on NASH would be difficult to observe in this model. Therefore, we tested the beneficial effect of alirocumab in a more severe NASH model induced by methionine- and choline-deficient (MCD) feeding. As expected, serum PCSK9 levels were high in the serum of CD-fed mice (~150 ng/mL), which was slightly increased in MCD-fed mice (Supplemental Figure 12A). Alirocumab treatment remarkably upregulated hepatic LDLR expression in both CD- and MCD-fed groups compared with their corresponding control groups (Figure 8B). Interestingly, RT-qPCR results showed that alirocumab treatment significantly increased hepatic miR-223 expression in CD-fed mice but not in MCD-fed mice (Supplemental Figure 12B). MCD diet feeding causes significant hepatic infiltration of neutrophils, which express much higher levels of miR-223 than hepatocytes (Supplemental Figure 3B), so the total liver miR-223 detected by RT-qPCR may not reflect the miR-223 expression in hepatocytes. To detect miR-223 in hepatocytes, we performed miR-223 in situ hybridization and found that miR-223 expression in hepatocytes was significantly elevated after alirocumab treatment compared with control treatment (Figure 8, C and D, and Supplemental Figure 12C), which is consistent with the lower expression of several known miR-223 target genes in hepatocytes in alirocumab-treated groups versus control groups (Figure 8E). Moreover, MCD-induced NASH-related features were significantly ameliorated after alirocumab treatment, as demonstrated by the reduction in steatosis, liver neutrophil and macrophage infiltration, fibrosis, serum ALT levels, and NAS, which were examined by H&E staining, immunostaining, and RT-qPCR analyses (Figure 9, A–C, and Supplemental Figure 13, A and B). In addition, alirocumab treatment increased the expression of the VLDL-related gene *Mttp* but not several β-oxidation–related genes, suggesting that induction of LDLR following alirocumab treatment may contribute to limiting liver injury by improving VLDL synthesis (Supplemental Figure 13C).

Discussion

Neutrophil infiltration is a hallmark of NASH and is believed to promote hepatocyte damage in NASH through the generation of reactive oxygen species and the production of proinflammatory mediators (37, 38). However, neutrophils may also play an important role in promoting liver fibrosis resolution via the production of miR-223 that inhibits macrophage activation (5). In the current study, we identified a selective, LDLR- and APOE-dependent EV transfer of neutrophil-derived miR-223 into hepatocytes, which plays a beneficial role in mitigating the progression of NAFLD (Figure 10).

The liver expresses very low levels of pri-miR-223. Mature miR-223 in the liver is mainly transferred from immune cells, as demonstrated by our BM transplantation experiments. Among these immune cells, neutrophils are probably the major source

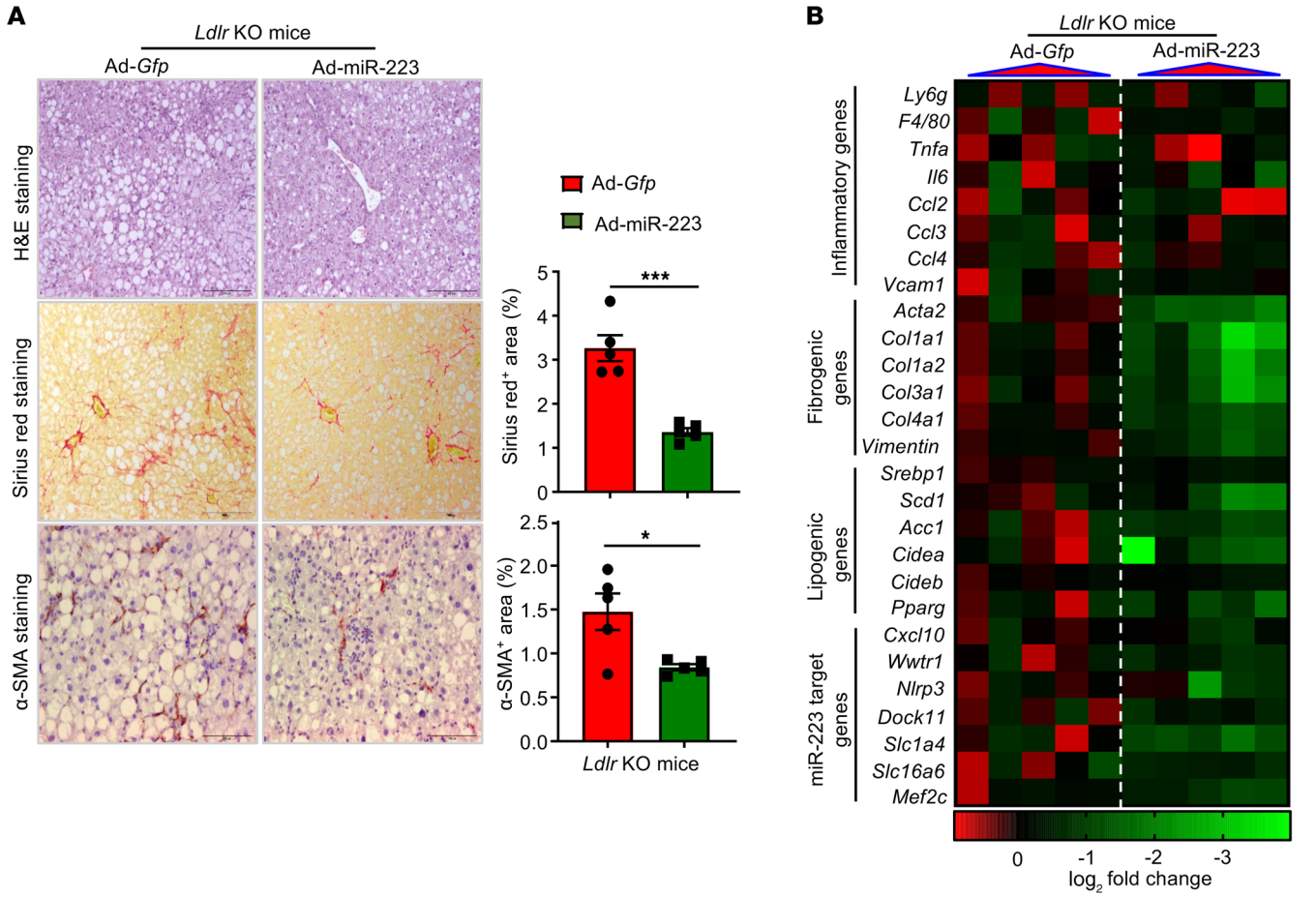

Figure 5. Restoration of hepatic miR-223 reverses NASH in HFD-fed *Ldlr*-KO mice. *Ldlr*-KO mice were fed HFD for 3 months with the intravenous injection of adenovirus-*Gfp* (Ad-*Gfp*) (n = 5) or Ad-miR-223 (n = 5) starting at 2 months for a total of 2 times (once every 2 weeks). Liver and serum samples were collected. (**A**) Representative images of H&E staining (scale bar: 200 μm), Sirius red staining (scale bar: 200 μm), and α-SMA staining (scale bar: 100 μm) of liver tissue sections are shown. Fibrotic area per field was quantified. (**B**) RT-qPCR analyses of several genes. Values represent means ± SEM. $^*P < 0.05$, $^{***}P < 0.001$, as determined by 2-tailed Student's t test for comparing 2 groups (**A**).

of miR-223 transfer into hepatocytes, while other types of cells, especially macrophages, may also contribute, albeit to a lesser extent. First, miR-223 is mainly expressed in myeloid cells, with the highest levels in neutrophils (6). Second, neutrophils are the most abundant myeloid cell type in the body. Third, chronic neutrophil depletion experiments revealed a reduction by approximately 30% of circulating neutrophils, which correlates well with a similar reduction in circulating miR-223. Future studies using neutrophil-specific miR-223KO mice may further test whether neutrophils are the major source of circulating miR-223. Here, we provide in vitro and in vivo evidence indicating that neutrophil-derived miR-223 is packaged in EVs and that transfer of these EVs is the primary source of miR-223 in hepatocytes. The in vitro evidence includes isolation and validation of miR-223–enriched EVs from neutrophils, coculture of hepatocytes and neutrophils in the presence or absence of an EV-release inhibitor, and hepatocyte uptake of neutrophil-derived EVs. Although it was challenging to obtain in vivo evidence for the transfer of neutrophil-derived miR-223 to hepatocytes via EVs, 2 experiments support this notion. First, fluorescence was detected in the liver (hepatocytes) after injection of fluorescently labeled neutrophil-derived EVs in mice. Second, miR-223 was detected in hepatocytes in miR-223KO mice after injection of neutrophil-derived, miR-223–enriched EVs.

One interesting finding from the current study is that the selective transfer of miR-223 into hepatocytes is dependent on LDLR in hepatocytes and APOE in neutrophils, and it plays an important role in preventing NAFLD progression. The liver is an active site of EV uptake and has tremendous capacity for rapid uptake and clearance of circulating EVs (39), which may account for the selective uptake of miR-223–enriched EVs in fatty liver but not in other organs. One of the reasons for the preferential EV uptake by hepatocytes is likely the existence of sinusoidal endothelial cell fenestrae (141 ± 5.4 nm in C57BL/6 mice, 107 ± 1.5 nm in humans) (40), which allows small EVs, such as exosomes of 30–150 nm in diameter, to pass through easily and interact with hepatocytes. Another mechanism uncovered in the current study is that high levels of LDLR in hepatocytes promote EV uptake; genetic deletion of *Ldlr* increased circulating miR-223–enriched EVs in HFD-fed mice, probably caused by their reduced transfer into hepatocytes, as suggested by their reduced levels in the liver. Direct evidence for LDLR-mediated EV uptake was provided

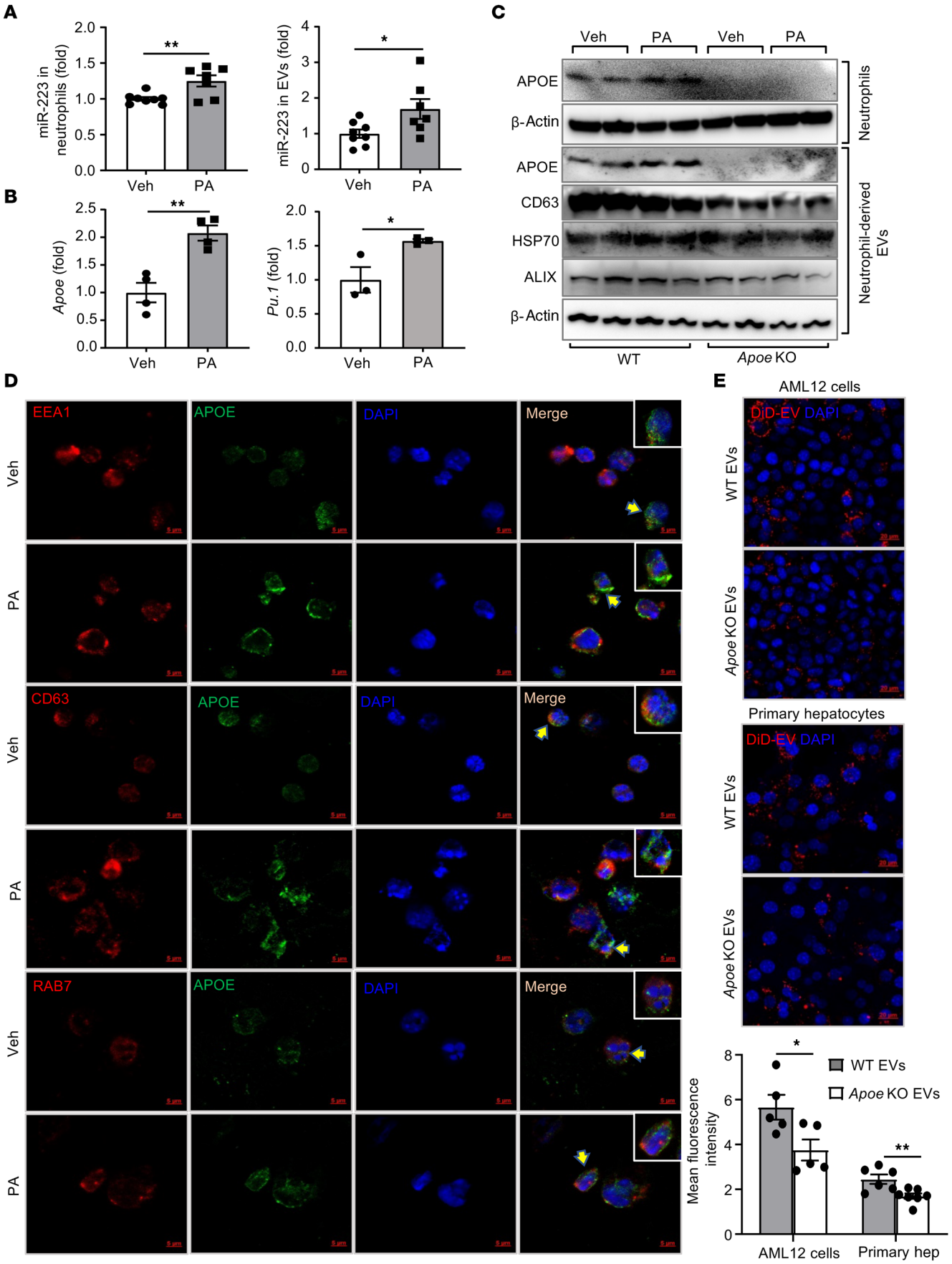
A
miR-223 in neutrophils (fold)
miR-223 in EVs (fold)
Veh
PA
B
Apoe (fold)
Pu.1 (fold)
C
Veh
PA
Veh
PA
APOE
β-Actin
Neutrophils
APOE
CD63
HSP70
ALIX
β-Actin
Neutrophil-derived EVs
WT
Apoe KO
D
EEA1
APOE
DAPI
Merge
CD63
RAB7
E
AML12 cells
DiD-EV DAPI
WT EVs
Apoe KO EVs
Primary hepatocytes
Mean fluorescence intensity
WT EVs
Apoe KO EVs
AML12 cells
Primary hep

Figure 6. PA induces neutrophils to release APOE-enriched EVs. Bone marrow neutrophils were cultured in serum-free medium and stimulated with vehicle or PA (0.3 mM) for 6 hours. (**A**) miR-223 levels in neutrophils and neutrophil-derived EVs were measured. (**B**) *Apoe* and *Pu.1* mRNA levels in neutrophils were measured. (**C**) Western blot analyses of APOE in bone marrow neutrophils and EV marker proteins in neutrophil-derived EVs from WT and *Apoe*-KO mice. (**D**) Colocalization of APOE with an early endosome marker (EEA1), EV marker (CD63), or late endosome marker (RAB7) was determined. Representative images of these markers (red), APOE (green), and nuclei (DAPI, blue) are shown. Scale bars: 5 μm. (**E**) AML12 cells and primary mouse hepatocytes were incubated with DiD-labeled EVs that were derived from serum-free–cultured neutrophils. Representative images of DiD (red) and nuclei (blue) are shown, and mean fluorescence intensity per cell was quantified (bottom). Scale bars: 20 μm. Values represent means ± SEM. $^{*}P < 0.05$, $^{**}P < 0.01$, as determined 2-tailed Student's *t* test for comparing 2 groups (**A**, **B**, and **E**).

by 3 lines of evidence. First, injection of fluorescently labeled EVs resulted in much lower hepatic EV uptake in *Ldlr*-KO mice than in WT mice. Second, *Ldlr*-deleted hepatocytes had a significantly reduced ability to take up neutrophil-derived, miR-223–enriched EVs in cell culture experiments. Finally, upregulation of LDLR by treatment with the PCSK9 inhibitor alirocumab promoted miR-223 transfer after coculture with neutrophils in vitro and after CD or MCD diet feeding in vivo. Surprisingly, genetic deletion of *Ldlr* did not affect hepatic miR-223 in CD-fed mice, probably because under control, lean conditions, pathways other than LDLR are involved in miR-223–enriched EV transfer. For example, high-density lipoprotein (HDL) receptor scavenger receptor class B type 1 (SR-B1) can take up miR-223–enriched HDL, which is increased in CD-fed *Ldlr*-KO mice (41, 42), which may compensate for the reduced LDLR-mediated miR-223 transfer. Although the current EV isolation techniques from blood samples are probably unable to completely remove lipoproteins because of their similar sizes, the EVs we used for in vitro uptake or in vivo injection experiments were purified from the in vitro–cultured, serum-free neutrophils, which were unlikely to contain lipoprotein particles. Because lipoprotein particles such as LDL and HDL are enriched with miR-223 in the serum (41), it is reasonable to speculate that LDLR promotes circulating miR-223 transfer into hepatocytes also via the uptake of LDL and HDL in addition to EV uptake in vivo.

Both APOB and APOE, which are ligands for LDLR, contribute to LDLR-mediated endocytosis of lipoproteins that are enriched with APOB and/or APOE. Here we found that APOE but not APOB was detected in neutrophils and neutrophil-derived EVs (neutrophils were cultured in serum-free medium to remove serum lipoprotein contamination). Direct in vitro evidence for the role of APOE in EV transfer is that EVs derived from *Apoe*-KO neutrophils were much less efficiently taken up by hepatocytes than those from WT neutrophils. There is also in vivo evidence obtained in WT mice transplanted with *Apoe*-KO BM, in which plasma LDL/HDL levels were not affected (43, 44) and neutrophil-derived miR-223–enriched EVs lacked APOE. These mice displayed a smaller increase in HFD-induced hepatic miR-223 levels, probably as a result of reduced transfer of miR-223–enriched EVs that lack APOE.

As hepatocytes express very low levels of miR-223, the LDLR- and APOE-mediated transfer of neutrophil-derived miR-223 via EVs is functional, as suggested by the reduced hepatic miR-223 but increased hepatic expression of miR-223 target genes (*Cxcl10*, *Nlrp3*, *Taz*, *Dock11*, *Slc1a4*, *Slc16a6*, and *Mef2c*) in *Ldlr*-KO, *Apoe*-KO, and $WT^{Apoe\ KO\ BM}$ mice. Some of these target genes (such as *Cxcl10*, *Nlrp3*, and *Taz)* are known to induce liver inflammation and fibrosis, thereby promoting NAFLD progression. For example, CXCL10 plays a pivotal role in the pathogenesis of NASH by regulating lipogenesis, oxidative stress, and macrophage chemotaxis (45, 46). NLRP3 acts as a central driver of inflammation via the activation of caspase 1 and release of proinflammatory cytokines in the development of NASH (47). Hepatic TAZ contributes to the critical process of steatosis-to-NASH progression by inducing Indian hedgehog (Ihh) production, which is a secretory factor that promotes hepatic stellate cell activation (48).

It is possible that the loss of miR-223 transfer into the liver may account for some unrecognized mechanisms involved in the accelerated NASH in *Ldlr*-KO and *Apoe*-KO mice after HFD feeding, which may involve disrupted lipid metabolism (49, 50). Indeed, restoration of hepatic miR-223 ameliorated HFD-induced NASH and its associated liver fibrosis in *Ldlr*-KO mice, whereas liver injury was not improved after restoration of hepatic miR-223 in HFD-fed *Ldlr*-KO mice. This may be because overexpression of miR-223 can directly enhance hepatocyte injury (51), which may counteract the beneficial effect of miR-223 on liver injury and result in no changes in serum ALT levels. Therefore, LDLR ameliorates the development of NASH not only via the reduction of LDL/cholesterol levels but also via the transfer of neutrophil-derived, miR-223–enriched EVs into hepatocytes.

PCSK9 robustly inhibits hepatic LDLR expression at the posttranscriptional level. PCSK9 inhibition, which upregulates LDLR, is currently being used as a second-line treatment for hypercholesterolemia (52). Interestingly, treatment with PCSK9 has been shown to ameliorate alcoholic fatty liver disease (53) and PCSK9 may be involved in NAFLD development in experimental models and patients (54). Although these beneficial effects may be partially attributed to the reduction in cholesterol, the present findings suggest that PCSK9 inhibition can ameliorate NAFLD via a mechanism independent of LDL cholesterol reduction, by enhancing the LDLR-dependent miR-223–enriched EV uptake by hepatocytes, which then inhibits liver inflammation and fibrosis. Statins, the most common cholesterol-lowering drugs used to reduce cardiovascular morbidity and mortality, have also been found to improve NAFLD/NASH (55). Statins' effects are mediated via the inhibition of HMG-CoA reductase, but they can also regulate LDLR and PCSK9 expression (56). It will be interesting to test whether statins affect LDLR-dependent, neutrophil-derived, miR-223–enriched EV transfer into hepatocytes, which may contribute to their beneficial effect on NAFLD. LDLR or PCSK9 mutations cause familial hypercholesterolemia that is also associated with NAFLD development (57, 58). Mutation-induced defects in LDLR may interfere with the LDLR-dependent, miR-223–enriched EV transfer, which may be one of the underlying mechanisms by which familial hypercholesterolemia predisposes to NAFLD progression (59).

In summary, the LDLR- and APOE-mediated EV transfer of miR-223 from neutrophils into hepatocytes plays an important

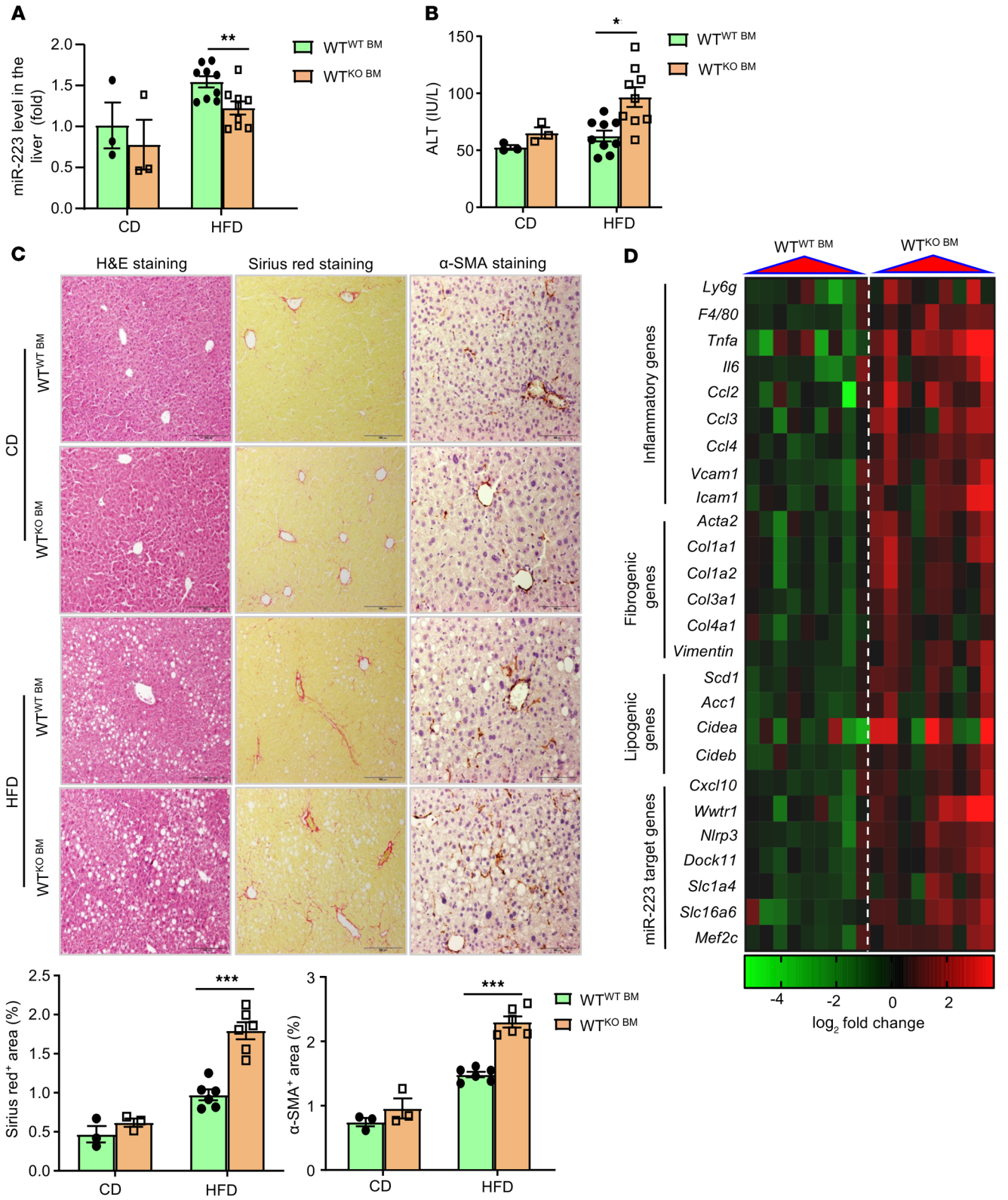

Figure 7. *Apoe* deficiency in immune cells worsens NASH partially due to less transfer of miR-223 to hepatocytes. WT mice were transplanted with WT or *Apoe*-KO mouse bone marrow (BM). The superscript characters indicate the donor mouse BM. Two months later, these mice were subjected to CD or HFD feeding for 3 months. Serum and liver tissue samples were collected ($n = 3$ in CD-fed group, $n = 9$ in HFD-fed group). (**A**) miR-223 in the liver was measured by RT-qPCR. (**B**) Serum ALT was measured. (**C**) Representative images of H&E staining (scale bars: 200 μm), Sirius red staining (scale bars: 200 μm), and α-SMA staining (scale bars: 100 μm) of liver tissue sections are shown. Fibrotic area per field was quantified (bottom). (**D**) RT-qPCR analyses of several genes in the liver tissues from HFD-fed mice. Values represent means ± SEM. $^*P < 0.05$, $^{**}P < 0.01$, $^{***}P < 0.001$. Significance was determined by 1-way ANOVA followed by Tukey's post hoc test for multiple groups (**A**) and a 2-tailed Student's *t* test for comparing 2 groups (**B** and **C**).

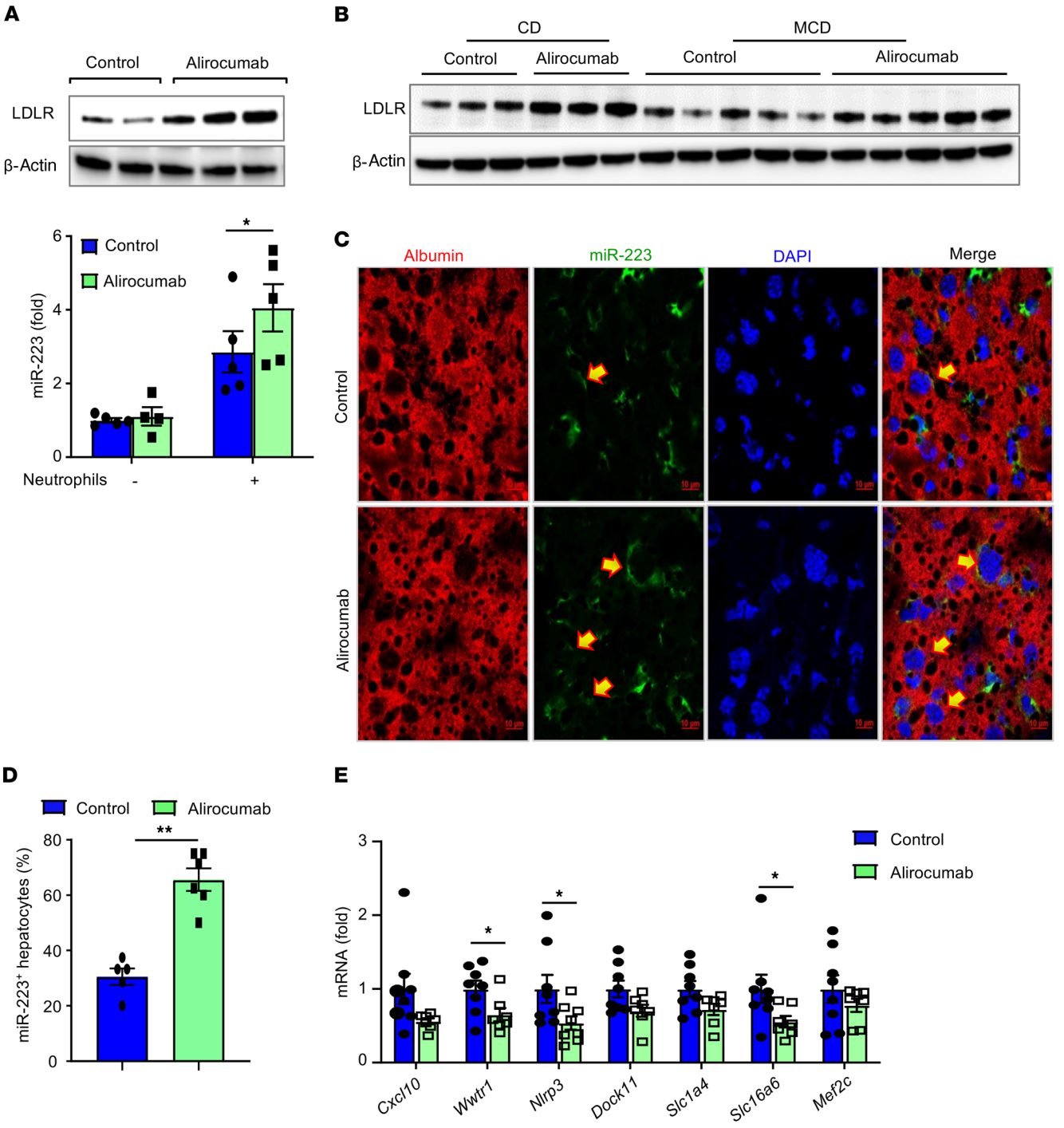

Figure 8. Administration of the PCSK9 inhibitor alirocumab enhances LDLR-dependent miR-223 transfer. (**A**) AML12 cells were pretreated with the PCSK9 inhibitor alirocumab or control antibody (10 μg/mL) for 24 hours, and then the cell medium was replaced with serum-free medium. LDLR expression in hepatocytes was measured by Western blotting (upper panel). These hepatocytes were cocultured with neutrophils for another 6 hours, and miR-223 levels in hepatocytes were measured by RT-qPCR (lower panel). (**B**–**E**) C57BL/6J mice were also fed an MCD diet or control diet (CD) for 6 weeks. After 2-week MCD diet feeding, these mice were subcutaneously injected with alirocumab or control antibody at the dose of 10 mg/kg once per week for another 4-week MCD diet feeding. Serum and liver samples were collected (n = 3 in CD-fed group, n = 8 in MCD-fed group). (**B**) Liver LDLR protein was measured. (**C**) Frozen liver tissue sections from MCD-fed mice were analyzed by miR-223 in situ hybridization along with immunofluorescence staining of the hepatocyte marker albumin. Representative images of miR-223 expression (green), albumin (red), and nuclei (DAPI, blue) are shown. Scale bars: 10 μm. (**D**) miR-223$^+$ hepatocytes were quantified in MCD-fed mice. (**E**) miR-223 target genes were measured by RT-qPCR in MCD-fed mice. Values represent means ± SEM. $^*P < 0.05$, $^{**}P < 0.01$. Significance was determined by 1-way ANOVA followed by Tukey's post hoc test for multiple groups (**A**) and a 2-tailed Student's t test for comparing 2 groups (**D** and **E**).

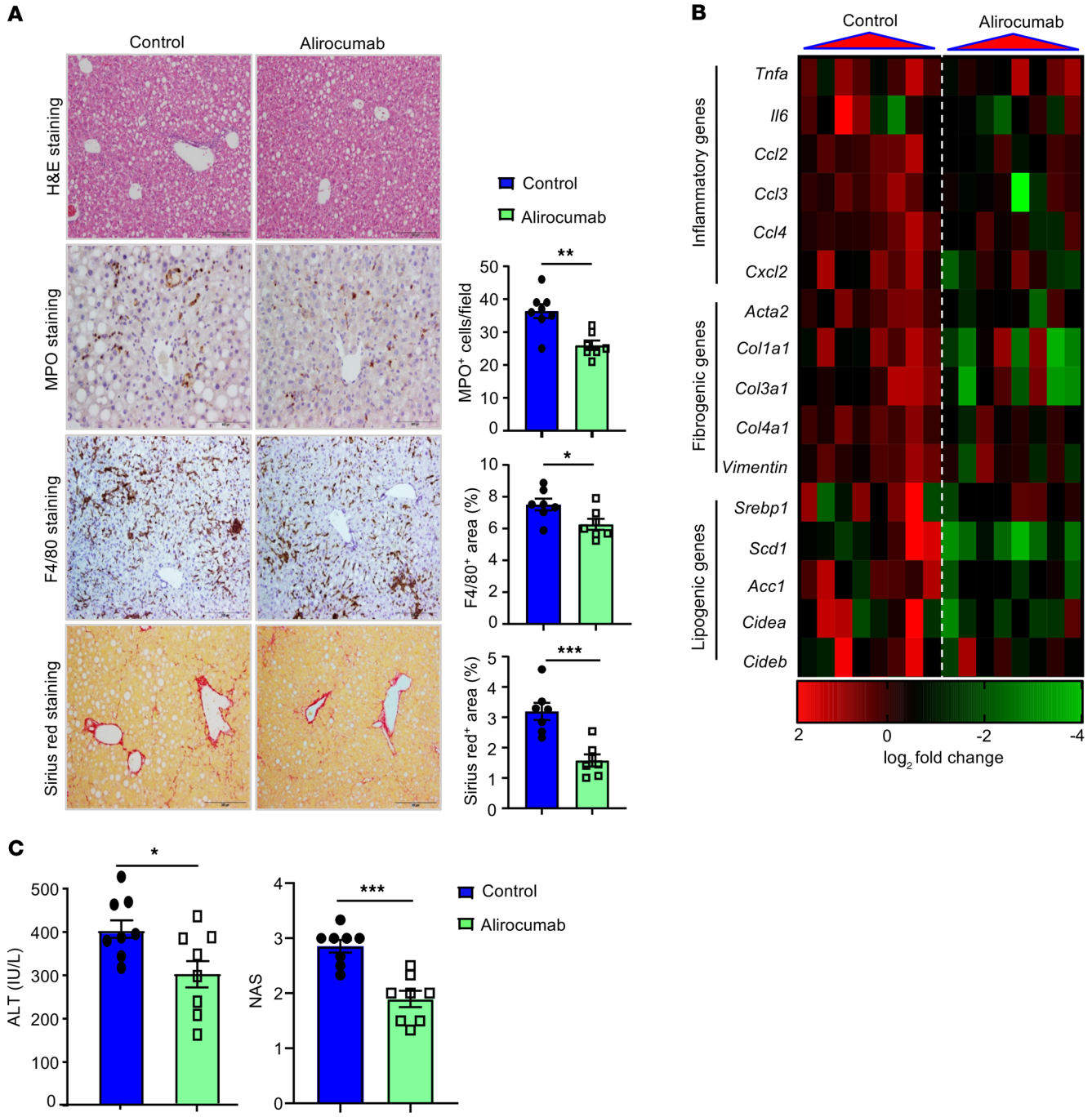

Figure 9. Administration of the PCSK9 inhibitor alirocumab ameliorates MCD-induced NASH by promoting LDLR-dependent miR-223 transfer. After 2-week MCD diet feeding, C57BL/6J mice were subcutaneously injected with alirocumab or control antibody at the dose of 10 mg/kg once per week for another 4-week MCD diet feeding. Serum and liver samples were collected (n = 8). (**A**) Representative images of H&E staining (scale bars: 200 μm), MPO staining (scale bars: 100 μm), F4/80 staining (scale bars: 200 μm), and Sirius red staining (scale bars: 200 μm) of liver tissue sections are shown. MPO$^+$ cells per field, F4/80$^+$ area, and fibrotic area per field were quantified. (**B**) RT-qPCR analyses of several genes in the liver. (**C**) Serum ALT levels and NAS were analyzed. Values represent means ± SEM. $^*P < 0.05$, $^{**}P < 0.01$, $^{***}P < 0.001$, as determined by 2-tailed Student's t test for comparing 2 groups (**A** and **C**).

role in preventing NAFLD progression due to the antiinflammatory and antifibrotic effect of miR-223. Of course, mechanisms other than miR-223 transfer may also contribute to LDLR/APOE regulation of NASH, such as LDL-related regulation of cholesterol levels, APOE-mediated antiinflammation, and LDLR induction–related VLDL synthesis. In addition to hepatocytes, other cell types can also take up neutrophil-derived, miR-223–enriched EVs, such as macrophages (5) and vascular endothelial cells (60–62), which likely play roles in controlling NASH progression. Finally, the clinical implication of this previously unrecognized role of LDLR and APOE in the selective control of EV uptake may contribute to the beneficial effect of PCSK9

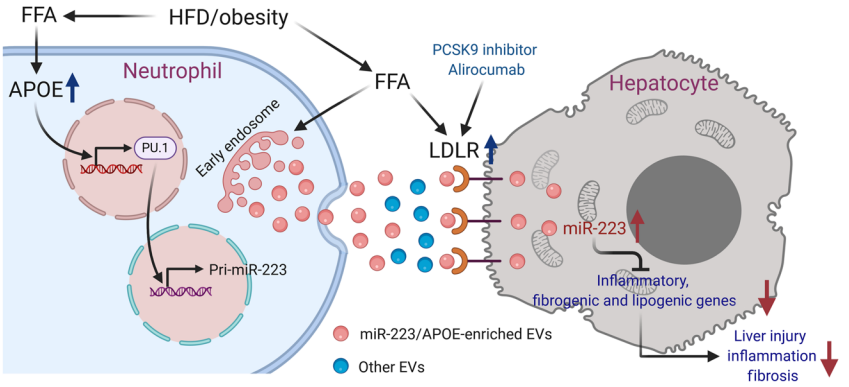

Figure 10. Scheme depicting a selective LDLR- and APOE-dependent EV transfer of neutrophilic miR-223 into hepatocytes and its role in the progression of NAFLD. In obesity, free fatty acids (FFAs) elevate miR-223 expression in neutrophils by regulating APOE/PU.1 signaling and miR-223 subsequently forms a feedback loop to prevent NASH progression by amplifying the preferential uptake of neutrophil-derived and antiinflammatory miR-223/APOE-enriched EVs in hepatocytes. This selective uptake is dependent on the expression of LDLR on hepatocytes and APOE on neutrophil-derived EVs. Upregulation of LDLR by treatment with the PCSK9 inhibitor alirocumab ameliorates NASH partially due to the augmentation of this miR-223 transfer.

inhibition on NALFD and may help us better understand the physiological and pathological functions of LDLR and APOE in the body. Additionally, recent phase III trials revealed that treatment with the PCSK9 inhibitor inclisiran effectively reduced blood LDL cholesterol levels in patients who failed to respond to statin therapy (63). Given an important role of hepatic miR-223 in controlling cholesterol homeostasis (64), our findings that LDLR/PCSK9 inhibition promotes miR-223–enriched EV uptake by hepatocytes may provide different insights into the mechanisms of LDLR/PCSK9 regulation of LDL cholesterol homeostasis, which may help design a better therapeutic strategy to treat patients with PCSK9 inhibitors.

Methods

Mice. miR-223KO (stock number 013198), *Ldlr*-KO (stock number 002207), *Apoe*-KO (stock number 002052), and *Cd36*-KO (stock number 019006) mice were purchased from The Jackson Laboratory. Male miR-223$^{-/y}$ (KO) and littermate miR-223$^{+/y}$ (WT) mice were obtained via the breeding of male miR-223$^{-/y}$ and female miR-223$^{+/-}$ mice, as described in our previous study (11).

For HFD feeding, male mice were fed an HFD (60 kcal% fat; catalog no. D12492, Research Diets, Inc.) or a chow diet (10 kcal% fat) as a CD for 3 months.

For adenovirus-mediated expression, *Ldlr*-KO mice were fed an HFD for 3 months. In the last month, these mice were administered 2 tail vein injections (once per 2 weeks) with adenovirus expressing mouse miR-223 (Ad-miR-223) (Vector Biolabs) or GFP (Ad-*Gfp*) (Vector Biolabs) as a control.

For PCSK9 inhibitor (alirocumab) treatment, C57BL/6J mice (The Jackson Laboratory, stock number 000664) were also fed an MCD diet (MP Biomedicals, catalog 0296043920) or MCD control diet (MP Biomedicals, catalog 0296044110) for 6 weeks. After 2-week diet feeding, these mice were subcutaneously injected with alirocumab or control inhibitor at the dose of 10 mg/kg once per week for another 4-week CD or MCD diet feeding. Alirocumab was purchased from Regeneron Pharmaceuticals through the Division of Veterinary Resources at the NIH. Control inhibitor (anti-IgG, 10 mg/kg) was purchased from BioXCell.

Neutrophil depletion. The combined-antibody-mediated neutrophil depletion was performed as described recently (29). In brief, WT mice were fed with an HFD for 2.5 months, and then daily intraperitoneally injected with IgG2a isotype antibody (clone 2A3, catalog no. BP0089, BioXCell) or combined antibodies (anti-Ly6G [clone 1A8, catalog no. BP0075-1, BioXCell] and anti-rat secondary antibody [clone MAR 18.5, catalog no. BE0122, 100 μg/mouse, BioXCell]) for 18 days. For isotype antibody and anti-Ly6G antibody injection, 50 μg/mouse was used in the first week, and then 100 μg/mouse for subsequent injection. When mice were sequentially injected with combined antibodies, we incorporated a 2-hour delay between injections. Liver and serum samples were collected 24 hours after the last injection.

Isolation and labeling of EVs, and EV uptake assay. For serum EV isolation, serum samples were precleared to remove the lipoprotein particles by using proprietary precleaning reagents and EVs were purified by using ExoQuick-LP solution (System Biosciences) according to the manufacturer's instructions. The purified serum samples were mixed with ExoQuick solution and incubated at 4°C overnight, followed by centrifuging at 14,000 rpm for 10 minutes. The final pellets containing EVs were collected for further study.

EVs in the cell medium were isolated by using ExoQuick-TC solution (System Biosciences) according to the manufacturer's instructions. The EV pellet was dissolved in phosphate-buffered saline (PBS), and then was labeled using the red-fluorescent dye DiD, which stains cell membranes and lipids (Thermo Fisher Scientific) by following the manufacturer's instructions at a 1:200 dilution. Briefly, EVs were incubated with 1 mL DiD solution for 15 minutes and then subjected to ultracentrifugation at 100,000*g* for 70 minutes at 4°C to remove free DiD dye. The labeled EVs were resuspended in PBS and rotated at 4°C overnight and finally used as the EV fraction. For EV lysis, neutrophil-derived EVs were treated with 0.1% Triton X-100 (Sigma-Aldrich) for 30 minutes at room temperature. For EV treatment, the seeded hepatocytes were pretreated with PA (0.3 mM) for 18 hours, and then the cell medium was changed to fresh medium. The EV fraction was added to the medium and after 24 hours the hepatocytes were fixed in 4% paraformaldehyde. The slides were incubated with primary antibodies against LDLR (catalog no. ab52818, Abcam) at 4°C overnight, and then with Alexa Fluor–conjugated secondary antibody (Alexa Fluor 488–goat anti–rabbit IgG [H+L], Cell Signaling Technology) for 1 hour at room temperature. The images were obtained by using an LSM 710 confocal microscope (Zeiss).

Statistics. Data are expressed as the mean ± SEM for each group and were analyzed using GraphPad Prism software. To compare values obtained from 2 groups, 2-tailed Student's *t* test was performed. Data from multiple groups were compared with 1-way ANOVA followed by Tukey's post hoc test. *P* values less than 0.05 were considered significant.

Study approval. All animal studies were approved by the NIAAA Animal Care and Use Committee.

Author contributions

YH designed and conducted the experiments and wrote the manuscript. RMR, XW, WS, JM, SH, YF, ET, CM, SZ, RR, and DF conducted some experiments and edited the manuscript. PP and GK assisted with data analysis and edited the manuscript. BG supervised the entire project and wrote the manuscript.

Acknowledgments

The authors want to thank Raouf Kechrid (NIAAA) for purchasing alirocumab and Falk Lohoff (NIAAA) for providing information for alirocumab treatment in mice. This work was supported by the intramural program of the NIAAA, NIH (to BG).

Address correspondence to: Bin Gao, MD, PhD, Laboratory of Liver Diseases, NIAAA/NIH, 5625 Fishers Lane, Bethesda, Maryland 20892, USA. Phone: 301.443.3998; Email: bgao@mail.nih.gov.

1. Friedman SL, et al. Mechanisms of NAFLD development and therapeutic strategies. *Nat Med*. 2018;24(7):908–922.
2. Rinella ME, et al. Report on the AASLD/EASL joint workshop on clinical trial endpoints in NAFLD. *Hepatology*. 2019;70(4):1424–1436.
3. Gao B, Tsukamoto H. Inflammation in alcoholic and nonalcoholic fatty liver disease: friend or foe? *Gastroenterology*. 2016;150(8):1704–1709.
4. Cai J, et al. The role of innate immune cells in nonalcoholic steatohepatitis. *Hepatology*. 2019;70(3):1026–1037.
5. Calvente CJ, et al. Neutrophils contribute to spontaneous resolution of liver inflammation and fibrosis via microRNA-223. *J Clin Invest*. 2019;129(10):4091–4109.
6. Ward JR, et al. Regulation of neutrophil senescence by microRNAs. *PLoS One*. 2011;6(1):e15810.
7. Li M, et al. MicroRNA-223 ameliorates alcoholic liver injury by inhibiting the IL-6-p47(phox)-oxidative stress pathway in neutrophils. *Gut*. 2017;66(4):705–715.
8. Wang X, et al. MicroRNAs as regulators, biomarkers and therapeutic targets in liver diseases [published online October 30, 2020]. *Gut*. https://doi.org/10.1136/gutjnl-2020-322526.
9. Yuan X, et al. MicroRNA miR-223 as regulator of innate immunity. *J Leukoc Biol*. 2018;104(3):515–524.
10. He Y, et al. Hepatic mitochondrial DNA/Toll-like receptor 9/microRNA-223 forms a negative feedback loop to limit neutrophil overactivation and acetaminophen hepatotoxicity in mice. *Hepatology*. 2017;66(1):220–234.
11. He Y, et al. MicroRNA-223 ameliorates nonalcoholic steatohepatitis and cancer by targeting multiple inflammatory and oncogenic genes in hepatocytes. *Hepatology*. 2019;70(4):1150–1167.
12. van Niel G, et al. Shedding light on the cell biology of extracellular vesicles. *Nat Rev Mol Cell Biol*. 2018;19(4):213–228.
13. Shah R, et al. Circulating extracellular vesicles in human disease. *N Engl J Med*. 2018;379(22):2180–2181.
14. Yáñez-Mó M, et al. Biological properties of extracellular vesicles and their physiological functions. *J Extracell Vesicles*. 2015;4:27066.
15. Li J, et al. Characterization of cellular sources and circulating levels of extracellular vesicles in a dietary murine model of nonalcoholic steatohepatitis. *Hepatol Commun*. 2019;3(9):1235–1249.
16. Hirsova P, et al. Lipid-induced signaling causes release of inflammatory extracellular vesicles from hepatocytes. *Gastroenterology*. 2016;150(4):956–967.
17. Neudecker V, et al. Neutrophil transfer of *miR-223* to lung epithelial cells dampens acute lung injury in mice. *Sci Transl Med*. 2017;9(408):eaah5360.
18. Mulcahy LA, et al. Routes and mechanisms of extracellular vesicle uptake. *J Extracell Vesicles*. 2014;3.
19. Murphy DE, et al. Extracellular vesicle-based therapeutics: natural versus engineered targeting and trafficking. *Exp Mol Med*. 2019;51(3):1–12.
20. Nanbo A, et al. Exosomes derived from Epstein-Barr virus-infected cells are internalized via caveola-dependent endocytosis and promote phenotypic modulation in target cells. *J Virol*. 2013;87(18):10334–10347.
21. Wei F, et al. Exosomes derived from gemcitabine-resistant cells transfer malignant phenotypic traits via delivery of miRNA-222-3p. *Mol Cancer*. 2017;16(1):132.
22. Weinreich M, Frishman WH. Antihyperlipidemic therapies targeting PCSK9. *Cardiol Rev*. 2014;22(3):140–146.
23. Goldstein JL, Brown MS. The LDL receptor. *Arterioscler Thromb Vasc Biol*. 2009;29(4):431–438.
24. Kockx M, et al. Cell-specific production, secretion, and function of apolipoprotein E. *J Mol Med (Berl)*. 2018;96(5):361–371.
25. Johnnidis JB, et al. Regulation of progenitor cell proliferation and granulocyte function by microRNA-223. *Nature*. 2008;451(7182):1125–1129.
26. Kalluri R, LeBleu VS. The biology, function, and biomedical applications of exosomes. *Science*. 2020;367(6478):eaau6977.
27. Gantier MP. The not-so-neutral role of microRNAs in neutrophil biology. *J Leukoc Biol*. 2013;94(4):575–583.
28. Stackowicz J, et al. Mouse models and tools for the in vivo study of neutrophils. *Front Immunol*. 2019;10:3130.
29. Boivin G, et al. Durable and controlled depletion of neutrophils in mice. *Nat Commun*. 2020;11(1):2762.
30. Goldberg IJ, et al. Regulation of fatty acid uptake into tissues: lipoprotein lipase- and CD36-mediated pathways. *J Lipid Res*. 2009;50 suppl(suppl):S86–S90.
31. Gupte AA, et al. Rosiglitazone attenuates age- and diet-associated nonalcoholic steatohepatitis in male low-density lipoprotein receptor knockout mice. *Hepatology*. 2010;52(6):2001–2011.
32. Loyer X, et al. Liver microRNA-21 is overexpressed in non-alcoholic steatohepatitis and contributes to the disease in experimental models by inhibiting PPARα expression. *Gut*. 2016;65(11):1882–1894.
33. Taibi F, et al. miR-223: An inflammatory oncomiR enters the cardiovascular field. *Biochim Biophys Acta*. 2014;1842(7):1001–1009.
34. Li K, et al. Apolipoprotein E enhances microRNA-146a in monocytes and macrophages to suppress nuclear factor-κB-driven inflammation and atherosclerosis. *Circ Res*. 2015;117(1):e1–e11.
35. Lagace TA, et al. Secreted PCSK9 decreases the number of LDL receptors in hepatocytes and in livers of parabiotic mice. *J Clin Invest*. 2006;116(11):2995–3005.
36. Farrell G, et al. Mouse models of nonalcoholic steatohepatitis: toward optimization of their relevance to human nonalcoholic steatohepatitis. *Hepatology*. 2019;69(5):2241–2257.
37. Hwang S, et al. Interleukin-22 ameliorates neutrophil-driven nonalcoholic steatohepatitis through multiple targets. *Hepatology*. 2020;72(2):412–429.
38. Kolaczkowska E, Kubes P. Neutrophil recruitment and function in health and inflammation. *Nat Rev Immunol*. 2013;13(3):159–175.
39. Szabo G, Momen-Heravi F. Extracellular vesicles in liver disease and potential as biomarkers and therapeutic targets. *Nat Rev Gastroenterol Hepatol*. 2017;14(8):455–466.
40. Wisse E, et al. The size of endothelial fenestrae in human liver sinusoids: implications for hepatocyte-directed gene transfer. *Gene Ther*. 2008;15(17):1193–1199.
41. Vickers KC, et al. MicroRNAs are transported in plasma and delivered to recipient cells by high-density lipoproteins. *Nat Cell Biol*. 2011;13(4):423–433.
42. Ishibashi S, et al. Hypercholesterolemia in low density lipoprotein receptor knockout mice and its reversal by adenovirus-mediated gene delivery. *J Clin Invest*. 1993;92(2):883–893.
43. Fazio S, et al. Increased atherosclerosis in mice reconstituted with apolipoprotein E null macrophages. *Proc Natl Acad Sci U S A*. 1997;94(9):4647–4652.
44. Van Eck M, et al. Accelerated atherosclerosis in C57BL/6 mice transplanted with ApoE-deficient bone marrow. *Atherosclerosis*. 2000;150(1):71–80.
45. Zhang X, et al. CXCL10 plays a key role as an inflammatory mediator and a non-invasive biomarker of non-alcoholic steatohepatitis. *J Hepatol*. 2014;61(6):1365–1375.
46. Ibrahim SH, et al. Mixed lineage kinase 3 mediates release of C-X-C motif ligand 10-bearing chemotactic extracellular vesicles from lipotoxic hepatocytes. *Hepatology*. 2016;63(3):731–744.
47. Knorr J, et al. The NLRP3 inflammasome in alcoholic and nonalcoholic steatohepatitis. *Semin Liver Dis*. 2020;40(3):298–306.

48. Wang X, et al. Hepatocyte TAZ/WWTR1 promotes inflammation and fibrosis in nonalcoholic steatohepatitis. *Cell Metab*. 2016;24(6):848–862.
49. Wouters K, et al. Dietary cholesterol, rather than liver steatosis, leads to hepatic inflammation in hyperlipidemic mouse models of nonalcoholic steatohepatitis. *Hepatology*. 2008;48(2):474–486.
50. Van Rooyen DM, et al. Hepatic free cholesterol accumulates in obese, diabetic mice and causes nonalcoholic steatohepatitis. *Gastroenterology*. 2011;141(4):1393–1403, 1403.e1–e5.
51. Qadir XV, et al. miR-223 deficiency protects against fas-induced hepatocyte apoptosis and liver injury through targeting insulin-like growth factor 1 receptor. *Am J Pathol*. 2015;185(12):3141–3151.
52. Stoekenbroek RM, et al. Inhibiting PCSK9 — biology beyond LDL control. *Nat Rev Endocrinol*. 2018;15(1):52–62.
53. Lee JS, et al. PCSK9 inhibition as a novel therapeutic target for alcoholic liver disease. *Sci Rep*. 2019;9(1):17167.
54. Theocharidou E, et al. The role of PCSK9 in the pathogenesis of non-alcoholic fatty liver disease and the effect of PCSK9 inhibitors. *Curr Pharm Des*. 2018;24(31):3654–3657.
55. Athyros VG, et al. Statins: an under-appreciated asset for the prevention and the treatment of NAFLD or NASH and the related cardiovascular risk. *Curr Vasc Pharmacol*. 2018;16(3):246–253.
56. Nozue T. Lipid lowering therapy and circulating PCSK9 concentration. *J Atheroscler Thromb*. 2017;24(9):895–907.
57. Hobbs HH, et al. Molecular genetics of the LDL receptor gene in familial hypercholesterolemia. *Hum Mutat*. 1992;1(6):445–466.
58. Abifadel M, et al. Mutations in PCSK9 cause autosomal dominant hypercholesterolemia. *Nature genetics*. 2003;34(2):154–156.
59. Moutzouri E, et al. Hypocholesterolemia. *Curr Vasc Pharmacol*. 2011;9(2):200–212.
60. Li S, et al. MicroRNA-223 inhibits tissue factor expression in vascular endothelial cells. *Atherosclerosis*. 2014;237(2):514–520.
61. Tabet F, et al. HDL-transferred microRNA-223 regulates ICAM-1 expression in endothelial cells. *Nat Commun*. 2014;5:3292.
62. Shi L, et al. MicroRNA-223 antagonizes angiogenesis by targeting β1 integrin and preventing growth factor signaling in endothelial cells. *Circ Res*. 2013;113(12):1320–1330.
63. Ray KK, et al. Two phase 3 trials of inclisiran in patients with elevated LDL cholesterol. *N Engl J Med*. 2020;382(16):1507–1519.
64. Vickers KC, et al. MicroRNA-223 coordinates cholesterol homeostasis. *Proc Natl Acad Sci U S A*. 2014;111(40):14518–14523.